# Cost Effective Off-Grid Automatic Precipitation Samplers for Pollutant and Biogeochemical Atmospheric Deposition

Alessia A. Colussi[1], Daniel Persaud[1], Melodie Lao[1], Bryan K. Place[2,‡], Rachel F. Hems[2,§], Susan E. Ziegler[3], Kate A. Edwards[4,ǂ], Cora J. Young[1,2], and Trevor C. VandenBoer[1,3]

[1] *Department of Chemistry, York University, Toronto, ON*
[2] *Department of Chemistry, Memorial University, St. John's, NL*
[3] *Department of Earth Science, Memorial University, St. John's, NL*
[4] *Canadian Forest Service, Natural Resources Canada, Corner Brook, NL*

‡ Now at: *SciGlob Instruments & Services LLC, Columbia, MD, USA*
§ Now at: *Department of Chemistry and Biochemistry, Oberlin College and Conservatory, OH, USA*
ǂ Now at*: Climate Change Impacts and Adaptation Division, Lands and Minerals Sector, Natural Resources Canada, Ottawa, ON*

**Correspondence:** Trevor VandenBoer (tvandenb@yorku.ca)

## Abstract

An important transport process for particles and gases from the atmosphere to aquatic and terrestrial environments is through dry and wet deposition. An open-source, modular, off-grid, and affordable instrument that can automatically collect wet deposition samples allows for more extensive deployment of deposition samplers in fieldwork and would enable more comprehensive monitoring of remote locations. Precipitation events selectively sampled using a conductivity sensor powered by a battery-based supply are central to off-grid capabilities. The prevalence of conductive precipitation - that which initially contains high solute levels and progresses through trace level concentrations to ultrapure water in full atmospheric washout, depends on the sampling location but is ubiquitous. This property is exploited here to trigger an electric motor via limit switches to open and close a lid resting over a funnel opening. The motors are operated via a custom-built and modular digital logic control board, which have low energy demands. All components, their design and rationale, and assembly are provided for community use. The modularity of the control board allows operation of up to six independent wet deposition units,

such that replicate measurements (e.g., canopy throughfall) or different collection materials for various targeted pollutants can be implemented as necessary.

We demonstrate that these platforms are capable of continuous operation off-grid for integrated monthly and bimonthly collections performed across the Newfoundland and Labrador Boreal Ecosystem Latitudinal Transect (47° to 53° N) during the growing seasons of 2015 and 2016. System performance was assessed through measured power consumption from 115 volts of alternating current (VAC; grid power) or 12 volts of direct current from battery supplies during operation under both standby (40 or 230 mA, respectively) and in-use (78 or 300 mA, respectively) conditions. In the field, one set of triplicate samplers was deployed in the open to collect incident precipitation (open fall) while another set was deployed under the experimental forest canopy (throughfall). The proof-of-concept systems were validated with basic measurements of rainwater chemistry including: i) pH ranging from 4.14 to 5.71 in incident open fall rainwater; ii) conductivity ranging from 21 to 166 µS/cm; and iii) dissolved organic carbon concentrations in open fall and canopy throughfall of 16 ± 10 mg/L and 22 ± 12 mg/L, respectively; with incident fluxes spanning 600 to 4200 mg C $m^{-2}$ $a^{-1}$ across the transect. Ultimately, this demonstrates that the customized precipitation sampling design of this new platform enables more universal accessibility of deposition samples to the atmospheric observation community – for example, those who have made community calls for targeting biogeochemical budgets and/or contaminants of emerging concern in sensitive and remote regions.

## 1.0 Introduction

Atmospheric deposition is the central loss process for particles and gases to terrestrial and aquatic surfaces (Pacyna, 2008). Particles and gases can be deposited by both dry and wet deposition processes. Dry deposition is facilitated by the direct interaction of gases and particles with boundary layer surfaces such as water, vegetation, and/or soil, while wet deposition involves in-cloud scavenging and below-cloud interception of gases and aerosols by, e.g., rain droplets and snow crystals (Fowler, 1980; Lovett and Kinsman, 1990). Dry and wet deposition are global processes coupled to regional synoptic scale conditions, but their relative importance depends on local sources and global transport of atmospheric analytes of interest. Dry deposition consists of a variety of mechanisms for particles and gases, with fine mode particles and their chemical constituents (compared to ultrafine and coarse mode particles) being more likely to undergo

atmospheric long-range transport prior to being deposited (Farmer et al., 2021). Wet deposition occurs when such long-lived atmospheric particles and gases are included and/or scavenged into cloud water and transported to the surface of the Earth in precipitation (e.g., snow and rain). With the size and number of droplets in the atmosphere largely controlling the rate, wet deposition depends on a variety of meteorological factors affecting precipitation, such as the size distribution and concentration of ice and droplet nucleating particles, as well as the solubility, concentration, and reactivity of gases (Lovett, 1994). Ultimately, deposition plays an important role in pollutant distribution and biogeochemical cycling of long-studied major nutrients (e.g., nitrogen and sulfur in acid rain) and those with increasing recognition of importance such as dissolved organic carbon (DOC) (Meteorological Service of Canada, 2005; Vet et al., 2014; Safieddine and Heald, 2017; United States Environmental Protection Agency, 2020).

Recognizing the significance of atmospheric trace chemical deposition has led to the establishment of monitoring networks. For example, long-term wet deposition monitoring networks, like the Canadian Air and Precipitation Monitoring Network (CAPMoN) and the National Atmospheric Deposition Program (NADP), aim to provide critical data on the spatial and temporal patterns of wet and dry deposition. As a result, this has allowed for the estimation of regional and continental deposition rates of species regulated by national or international policies (Lovett, 1994). Data from these networks have been critical to understanding the efficacy of policy to reduce environmental issues like acid rain (Likens and Butler, 2020). In particular, the Oslo and Geneva protocols have achieved an 80% decrease in both North American and European $SO_2$ emissions since 1980 (Grennfelt et al., 2020). Despite these successes, reduction in acid deposition has had unexpectedly slow recovery in ecosystems leaving them sensitized – necessitating continued deposition monitoring (Stoddard et al., 1999; Kuylenstierna et al., 2001).

**Over the past 60 years, the precipitation chemistry community has made advancements in deposition collectors to better understand atmospheric processes (Siksna, 1959).** While bulk deposition collection (i.e., a collection bucket or jug fitted with a funnel open at all times; Hall, 1985) is both a simple and economically feasible sampling method utilized by monitoring networks, it is subject to bias through collection of inputs other than atmospheric deposition (e.g., bird droppings, insects, plant debris). As a result, bulk collectors can overestimate total deposition and underestimate wet deposition in a variety of locations (Lindberg et al., 1986; Richter and Lindberg, 1988; Stedman et al., 1990). **Sequential precipitation collection methods**

include manually segmenting samplers (requiring only a shelter, clean surface, and an operator), linked collection vessels (sample containers that are filled in sequence via gravitational flow), amongst others and have been developed to analyze rainwater composition and measure parameters such as pH and conductivity (Gatz et al., 1971; Reddy et al., 1985; Vermette and Drake, 1987; Laquer, 1990). Sequential sampler designs have also been adapted to collect precipitation in remote field sites (Germer et al., 2007; Sanei et al., 2010). Although it is a more costly and time intensive method when compared to bulk deposition collection, the major appeal of measuring isolated wet deposition is the ability to isolate this individual atmospheric process. Further innovation can reduce bias and improve the preservation of samples, such as the use of sensors to automate isolation of collected precipitation or the addition of polymeric mesh barriers to reduce debris input in windy environments (Lovett, 1994) - yet commercial solutions often come at a substantial expense.

When targeting biogeochemically relevant species in deposition collectors, additional standard practices have been developed to improve the representativeness of sample composition. First, an appropriate monitoring site must be selected. Three categories of siting criteria, established by organizations such as CAPMoN and the NADP, are of particular importance: (i) site representativeness and physical characteristics, (ii) distance from potential pollution sources, and (iii) operational requirements (Canadian Air and Precipitation Monitoring Network, 1985a; National Atmospheric Deposition Program, 2009). This means that each site must be a location that receives precipitation representative of the hydrologic area; is ideally not within 500 m of local pollution sources, such as wood-burning stoves, garbage dumps, and vehicle parking lots; and is accessible for daily collections, maintenance, and can be serviced by reliable 115 volts of alternating current (VAC) electrical power (Canadian Air and Precipitation Monitoring Network, 1985a; National Atmospheric Deposition Program, 2009). Despite these guidelines, there are many reasonable scenarios in which these siting conditions cannot be met. As an example, remote sample collections are often required for global assessments on persistent contaminants or nutrients of biogeochemical importance. Remote locations, however, can result in sampling sites with no power provision, infrequent sample collection, and/or the infrastructure-bearing location itself being a source of the targeted pollutants. As a result, innovation in collection strategies such as time-integrated off-grid sampling, with modularity in the deployment of replicates, as well as

materials for quantitative collection of environmental targets, is still needed to expand and/or modify networks to meet current and future monitoring and policy needs.

In biogeochemical cycles, for example, improvement of constraints in atmospheric carbon linkages to terrestrial and aquatic processes is necessary. This would play a critical role in correctly assessing climate feedbacks and reducing uncertainty in Earth system models. The measurement of atmospheric DOC transport to surfaces has been limited and impedes landscape scale carbon balance from being obtained (Casas-Ruiz et al., 2023). The pool of compounds from which DOC is derived in the atmosphere has also been limited and is only recently seeing an increase in research intensity. Reactive organic carbon (ROC) is defined as the sum of nonmethane organic gases and primary and secondary organic aerosols (Safieddine and Heald, 2017). The major removal mechanism of water-soluble organic compounds produced through oxidation from the atmosphere is by dry deposition of particle-bound pollutants and scavenging by rainfall (Jurado et al., 2004, 2005). When ROC is scavenged into rainfall, it becomes DOC and enters terrestrial and aquatic systems. Deposition measurements of ROC compounds are needed since they play a crucial role in the formation of secondary species such as ozone, particulate matter, and carbon dioxide ($CO_2$) (Safieddine and Heald, 2017; Heald and Kroll, 2020).

There are several evolving drivers around studying atmospheric ROC; for example, light-absorbing organic carbon that can affect global radiative balance and undergo photochemical transformations in the condensed phase (Saleh, 2020; Wang et al., 2021; Washenfelder et al., 2022; George, 2023). Reactive organic carbon can also influence cloud formation and contribute to precipitation acidity (Avery et al., 2006; Ramanathan and Carmichael, 2008). Measurements of speciated ROC are difficult due to the chemical complexity of emitted compounds and oxidation products (Heald and Kroll, 2020). To circumvent this, monitoring and quantifying DOC can be used as a proxy to estimate the total ROC in precipitation. However, quantitative measurements of DOC in precipitation samples are sparse due to its relatively low concentration of 0.1 to 10 mg C $L^{-1}$ (Iavorivska et al., 2016; Safieddine and Heald, 2017). Recently, calls for carbon closure on atmospheric processing of ROC make this measurement of increasing importance (Kroll et al., 2011; Heald et al., 2020; Barber and Kroll, 2021). Similarly, to obtain net landscape or watershed carbon exchange, studies require effective methods for capturing and preserving atmospheric DOC deposition to constrain biogeochemical linkages at global interfaces as outlined above.

In this work, we present the design of a custom-built automated array of precipitation samplers that can be operated both on- and off-grid for wet deposition collection. The purpose of these samplers is to enable cost-effective collection of integrated water-soluble conductive atmospheric constituents deposited in remote environments without grid power or routine access. A sensor interfaces with a custom-built motor control board capable of operating up to six independent wet deposition units such that canopy throughfall (TF) and incident precipitation (open fall, OF) measurements are possible to collect in replicate. The materials used can be easily changed in order to optimize collection **and preservation** of a wide array of target analytes, such as DOC, **when using high density polyethylene and mercuric chloride ($HgCl_2$).** We demonstrate that these platforms are capable of continuous operation off-grid for monthly wet deposition collection of precipitation across the Newfoundland and Labrador Boreal Ecosystem Latitudinal Transect (NL-BELT) during snow-free periods in 2015 and 2016. Extremes in system performance were evaluated by testing the power consumption of a sampling array from spring through fall when paired with a solar top-up system, and during snow-free winter conditions using only a battery. The two years of field samples were collected using an array of six collection units, with triplicate collection of both incident precipitation and throughfall from rain passing through a forest canopy. Samples were analyzed in terms of deposition volumes relative to total bulk volumes, reproducibility of replicate samples, and to determine the fraction of conductive rainfall within the total volume of precipitation at these remote sites. The captured fraction compared to total volume deposited is used to gain insight into how these samplers can limit analyte dilution effects and improve method detection limits**, such as rejecting 50% of the total volume delivered as ultrapure precipitation leading to a factor of two improvement**. Chemical parameters of pH, conductivity, and DOC fluxes **collected according to established preservation protocols** were then **compared to prior measurements** to validate this proof-of-concept system. Measurement methods for pH and conductivity of rainwater are very well-established in the literature and serve as a baseline reference to ensure that the samples collected by the new devices presented in this work are consistent with what is expected in samples from a remote coastal environment, given the selective sampling strategy. We then move away from these well-established parameters to quantify DOC fluxes **using established biogeochemical preservation techniques for fresh water and groundwater** to demonstrate the potential of these samplers in

application to automated collection of analytes of emerging importance and interest in the remote locations of our latitudinal transect.

## 2.0 Materials and Methods

### 2.1 Precipitation Sampling Array Components

Each automated precipitation sampling setup can be operated as an array, here being used in groups of up to six collection units (Figure 1). A collection unit is a simple opaque doored box. The box protects the sample containers against exposure to direct sunlight and provides a mounting location for the funnel and lid, while also facilitating easy exchange of sample containers. The collection units can be fitted with stabilizing legs that allow them to be bolted to concrete or pinned by retaining rods when on soil. In both cases, this prevents tipping and loss of sample during high winds or wildlife-sampler interactions (e.g., Figures 2 and S1). The collection of precipitation is facilitated by a funnel mounted through the top of the sampling unit. The funnel tip extends into the opening of the sample collection container placed inside. The connection can be sealed to better preserve volatile analytes with tubing that passes through a sealed grommet (P/N 9280K34, McMaster-Carr) to enter the sample collection container and minimize evaporative losses. Precipitation events are sampled selectively by modulating the position of a lid over the funnel with an electric motor. The collection unit motors are operated by a digital control board, which interfaces with a precipitation sensor and requires 12 volts of direct current (VDC) power supplied to this system. Switches detecting the lid position ensure complete opening or closure of the funnel mouth for each collection unit.

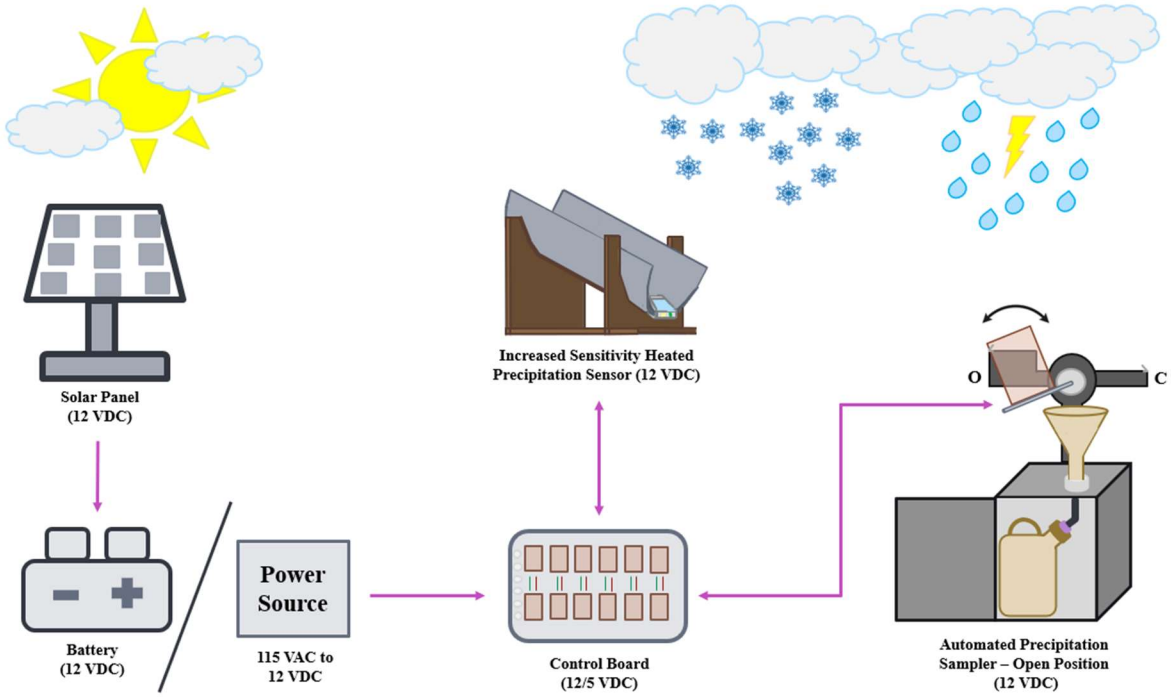


**Figure 1.** Schematic of custom-built automated precipitation sampling array components for off-grid wet deposition collection. The pink arrows denote the direction of electrical signal and power exchanged between components. The curved black arrow indicates the rotation of a motorized lid to obtain open (O) or closed (C) sampler configurations.

### 2.1.1 Collection Units

The collection unit materials to date have been made of both 3/8" plywood and black polyacrylate sheeting. The materials have demonstrated high durability on the order of four years under field conditions (Figures S1 and S2). Opaque materials were explicitly selected to minimize photochemical reactions and growth of photosynthetic microorganisms within the sample. The dimensions of the collection unit are detailed in Figure 2. Each can accommodate sample containers up to 20 L in volume for collection in locations with large monthly wet deposition volumes, such as in Newfoundland and Labrador (Table 1).

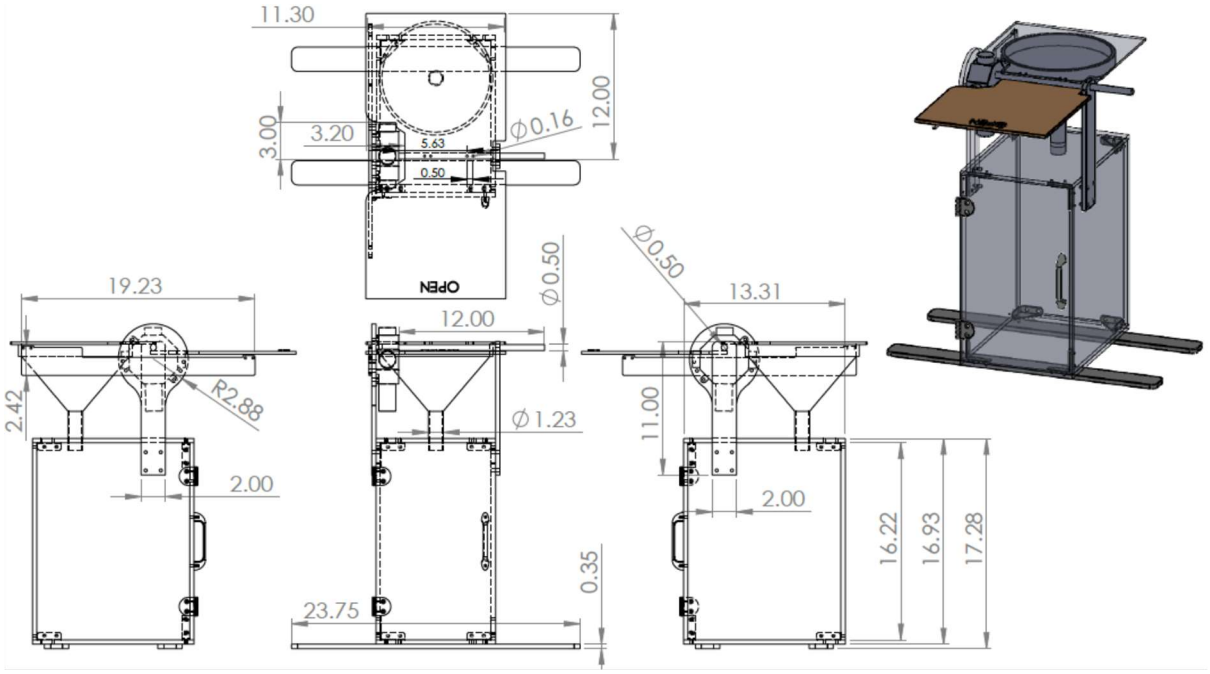


**Figure 2.** Detailed collection unit schematic with all dimensions provided in inches. Further specifications for the lid dimensions can be found in Figure S3. The shaded 3D rendering depicts both open and closed states for the lid, positioning of legs to secure it to surfaces, placement of corner brackets, and the door handle and hinges.

The box panels can be joined using hardware inserts (P/N 1556A54 and 1088A31, McMaster-Carr, Aurora, OH), 3D printed corners (Figure S4), or along the box edges with screws if using wood. The door is attached with two hinges (P/N 1549A57, McMaster-Carr) and held closed with a magnetic contact (P/N1674A61; McMaster-Carr) or hooked latch. The electric motor controlling the lid is enclosed in a standard polyvinylchloride electrical junction box, which is attached to a short paddle mounted on one side of the collection unit. Here we used an electric worm-gear motor (12 VDC, 2 revolutions per minute; TS-32GZ370-1650; Tsiny Motor Industrial Co., Dong Guan, China) mounted inside the enclosure with matching hex bolts (P/N 91251A146, McMaster-Carr) that passed through the weather-tight cover while the drive shaft protrudes through a 3/8" hole drilled in the cover. The drive shaft has a flat edge to affix the lid rod using a short set screw (Figure S5) that is cemented semi-permanently in place with thread locking compound (P/N 91458A112; Loctite Threadlocker Blue 242; McMaster-Carr). The lid rod is 3/8" aluminum machined on one end to allow connection to the motor drive shaft (Figure S5) with four threaded holes along its length to affix the lid (Figure S3). The lid rod passes through a second mounting paddle on the box that keeps the lid level and capable of isolating the funnel from the

atmosphere in the absence of precipitation. The lids used here were made of 1/8" Lexan polycarbonate sheet.

Selective precipitation sampling is performed using a logic-based assessment of sensor and switch states (defined in Figure S6) by the control board quadNOR gate chip (Fairchild Semiconductor P/N DM74LS02) which activates the H-bridge motor driver chipset (Figure S7). A 12 VDC signal drives the clockwise or counterclockwise rotation of the motor, installed in a suitable port of the junction box, via a cable from the control board, which passes through a weather-tight compression fitting (e.g., Home Depot SKU# 1000116446). The motor rotation signal is interrupted when the lid makes contact with one of two weather-tight limit switches (P/N SW1257-ND; Omron, Digi-Key Electronics, Thief River Falls, MN) mounted on opposite ends of a horizontal armature connected to the vertical motor mounting paddle (Figure 2). The switches controlling the lid location ensure that the funnel is completely open or covered as necessary for precipitation collection. The funnels used in this work are 20 cm in diameter and made from high-density polyethylene (HDPE; Dynalon, P/N 71070-020, VWR International, Mississauga, ON). A 7" x 5" piece of filtration mesh (P/N 9265T49, McMaster-Carr) that was tied together as a fitted cone insert with Nylon thread (e.g., fishing line) to prevent large debris entering the sampler containers when used, for example, in the collection of TF precipitation under a forest canopy when accompanying litterfall is also expected. The exit of the funnel directs the collected precipitation into the narrow-mouth opening the container inside the collection unit, such as 20 L HDPE jugs or 10 L HDPE jerricans (Bel-Art Products; P/N 11215-314, VWR International).

### 2.1.2 Heated Precipitation Sensor

The detection of rain modulates the opening and closing of the collection units by an interdigitated resistive sensor (M152; Kemo Electronic GmbH, Geestland, Germany; Figures S6 to S8). **This approach is consistent with established precipitation detection techniques used by government monitoring programs (e.g., CAPMoN; Canadian Air and Precipitation Monitoring Network, 1985a, 1985b).** The rain sensor detects conductive deposition by the completion of a conductive circuit when electrolytes bridge the connection between the interdigitated gold electrodes. The sensor is supplied with 12 VDC from the power system to trigger a relay when precipitation conductance above 1 MΩ·cm conductivity is detected (determined experimentally, see Section S1). **This is equivalent to approximately 8 µM sodium**

**chloride. The sensor detection limit reflects an upper limit of precipitation ion loading because the design of the rain chute leads to an increase in surface area of more than a factor of 25 on which solutes can accumulate to enhance the ionic content of the deposited water.** An output of 12 VDC is sent to the digital control board by the relay when rain is sensed, or 0 VDC in its absence, for signal processing and motor control (Figure S7). **When rain is sensed, the lid of each sampler in the array is simultaneously opened (<5 seconds) and is dependent on the rotational rate of the lid motor.** To increase the sensitivity of this sensor and to extend the sampling duration when conductive atmospheric constituents are completely washed out of the atmosphere, a sloped tin chute (e.g., Home Depot SKU# 1001110514) was added to extend the surface of the rain sensor. The sensor was placed at the end of the chute and sealed in place with caulking to allow water droplets to move easily from the chute onto the sensor.

The angle of the chute can be adjusted to control the momentum of collected droplets so that they collect on the sensor surface and only flow off it when the rate of precipitation exceeds the sensor evaporation capability. When soil is available, two bent rods can be used to hold the chute at the optimized angle of 10° (Figure S2). They are inserted into the soil and the chute is affixed to the tops of the rods with zip ties passed through small holes drilled in the sides of the chute, which are subsequently sealed with caulking. When soil is unavailable, for example in urban environments, we have created a mounting frame to hold the chute at the optimized angle of 10° (Figure S8). When precipitation is detected the sensor surface draws current up to 1.0 ampere (A) into a heater to actively evaporate water from its surface so that it accurately detects the active period of rain events. The heated sensor has undergone preliminary field tests and is also capable of detecting ice and snow, provided they contain electrolytes.

### 2.1.3 Power Supply Systems

Power for this system can be supplied from a battery at 12 VDC or using a 115 VAC to 12 VDC transformer power supply (P/N 285-1818-ND; TDK-Lambda Americas, Digi-Key Electronics). Depending on the duration of sampling and the time of year, the battery capacity can be changed to suit power needs (Section 3.2.2). To provide sufficient power density in this study, over one to two month-long collection periods, the battery capacity was carefully matched; with top-up options implemented when prolonged or high-frequency precipitation was expected. Absorbent glass mat (AGM) marine deep cycle batteries can withstand discharge events down to

less than 60 % capacity and are robust under nearly all environmentally relevant temperatures (≤ -20°C to 40°C). Additionally, these batteries interface easily with solar charging options as they are able to accept high current input. Monthly collections in Newfoundland were powered with 76 amp-hour (Ah) AGM batteries (Motomaster Nautilus; Ultra XD Group 24 High-Performance AGM Deep Cycle Battery, 12 VDC) topped up by a 40 W solar panel interfaced with a charge controller to prevent overcharging (Coleman; Model # 51840, max current of 8 A at 14 VDC).

For collections made every second month in Labrador, a 120 Ah battery with the same solar top-up strategy was used to ensure continuous operation. For either remote field deployment, batteries and charge controllers were housed in a Pelican™ case (Model 1440, Ocean Case Co. Ltd., Enfield, NS) fitted with weathertight bulkhead cord grips (P/N 7529K655, McMaster-Carr) through which charging and power cables were passed (Belden, Coleman; S/N 7004608, 70875227, Allied Electronics, Inc., Ottawa, ON). Humidity in all weatherproof cases was minimized by exchanging reusable desiccant packs (Ocean Case Co. Ltd.) when depleted batteries were exchanged for fully charged replacements. Solar panels were repositioned monthly to optimize orientation for solar power provision. Using either power source, the control board converts and distributes the 12 VDC to the other components in the precipitation sampling array.

### 2.1.4 Custom Control Board

A custom control board to operate a six-collection unit array was designed based on prior digital logic circuits for standalone collectors (VandenBoer, 2009). The 12 VDC battery or transformer output is supplied directly to the rain sensor and relay, as well as to the motor drivers for lid opening (Figure S9). Each collection unit is controlled independently to ensure lids are fully opened or closed, thereby requiring six replicate motor driver control circuits that respond to their independent switch signals. The remainder of the signaling and digital logic operates on 5 VDC which is produced by on-board voltage regulators (Micro Commercial Co; P/N MC7805CT-BP, Digi-Key Electronics). The lid switches are provided with 0 and 5 VDC to indicate collection unit open or closed status (Omron Electronics; P/N D2FW-G271M(D), Digi-Key Electronics). The signals from the sensor and switches connect to the board through four-conductor cable (Belden; S/N 70003678, Allied Electronics Inc.) passed through weathertight bulkhead cord grips and secured to screw terminals (Figure S9). The sensor and switch signal inputs interface with a quad NOR GATE chipset (Texas Instruments; P/N 296-33594-5-ND, Digi-Key Electronics) to trigger

the motor driver (STMicroelectronics; P/N 497-1395-5-ND, Digi-Key Electronics) such that it rotates or remains stationary. The additional resistors, capacitors, and diodes are necessary to maintain stable signaling throughout the printed circuit board (Figure S9, Table S1).

The custom control board was housed in a Pelican™ case (1400 NF; Pelican Zone, Mississauga, ON) fitted with cut-to-use foam inserts and a reusable desiccant pack that was also exchanged alongside those for the battery cases. All collection units, sensors, and power supply cables were passed through eight weathertight bulkhead cord grips and fixed to screw terminals on the board. The opposing ends of the cables were fitted with weathertight Bulgin Buccaneer 400 or 4000 Series circular cable connectors (Table S2; Allied Electronics, Inc.) to allow easy field installation with mated connectors on the cables originating from each of the previously mentioned array components. Connected cables could then be buried in shallow soil trenches to reduce the attention of gnawing animals, as well as potential entanglement hazards with other wildlife. Precipitation events were logged from the control boards using a HOBO 4-channel analog data logger (UX120-006M; Onset®, Bourne, MA) that records the sensor, switch, and motor voltages. The fourth channel is reserved to monitor battery or power supply voltages over time (Section 3.2).

**2.2 Power Demand and Management Tests**

Power demand was calculated based on the cumulative component requirements prior to the selection of batteries. This was to ensure adequate capacity to collect samples over one to two month-long field deployments and are sufficient for an assumed worst-case scenario of one week of constant rain without solar power charge restoration. Solar panel power production capacity was determined based on the calculated energy required to recharge the battery. As a result, we selected the 40 W panel which could complete charging at 14 VDC with a week of direct sunlight at 8 hours per day. The power demand for a six-sampler array was measured in standby and during operation with a digital power meter (Nashone PM90, Dalang Town, China) in real-time when supplying 12 VDC with a transformer. Contrasting power demand tests were performed under different environmental conditions and power management configurations. The first was performed using the 76 Ah AGM battery with a solar top-up in an urban environment from July through August 2018, while the other was performed using a 103 Ah AGM battery alone from January through February 2019.

## 2.3 Continuous Monthly Collection of Remote Samples at NL-BELT

One array of six automated collection units (3 OF, 3 TF) were deployed within one forested experimental field site located in each of the four watershed regions of the NL-BELT (24 samplers in total) between 2015 and 2016. Additionally, between one to three total deposition samplers were located at each of the four field sites (Table 1, Figure S10). The watersheds span 5.5° latitude from the southernmost site Grand Codroy (GC), through the colocated Pynn's Brook (PB) and Humber River Camp 10 (HR) sites, to Salmon River (SR) as the highest latitude site on the island of Newfoundland. The northernmost forested watershed, Eagle River (ER), is located in southern Labrador and extensive details characterizing each of the four sites can be found in Ziegler et al. (2017). All sampling locations are far from anthropogenic pollutant point sources, except for the ubiquitous presence of marine sea spray from the nearby marine coastlines. The total deposition samplers were identical to the automatic collection units except that they were not fitted with a motor arm and lid, so they did not require a source of power. Three of the six automated samplers were deployed in the open at a distance from the forest stand, equal to or greater than the height of the trees, in line with CAPMoN and NADP guidelines. The other three automated samplers were placed under the canopy to collect TF precipitation within the forest sites. These samplers actively collected wet deposition into integrated monthly (Newfoundland) or two-month (Labrador) samples during snow-free periods (approximately June through November). The arrays were collected and stored during the winter months while total deposition samplers remained in field locations year-round. It is also important to note that during the growing season, sample collections were made at the same time – that is, OF and TF deposition were collected on a single day at each sampling site and within a few days of each other across the transect. Collected sample volumes were compared between the automated samplers and total deposition collectors for each collection interval as a check on proper function (i.e., less than or equal volumes in automated samples). During each site visit, the slope of the sensor was confirmed to be correct, sample containers were collected and replaced with clean units, the battery and desiccant packs replaced with fully recharged devices, and the entire array confirmed operational.

**Table 1.** NL-BELT sampling site details provide locations and identifiers, alongside those from long-term weather stations operated by Environment and Climate Change Canada (ECCC). Soil pH was determined from samples collected at the same time as precipitation. Mean annual temperature was derived from ECCC climate normals. Annual total deposition precipitation

volumes were either measured for the 2015-16 period (ECCC, This Work) or calculated by the Oak Ridge National Lab DAYMET archive.

| Sampling Site | Sampling Site Location | Station (Climate ID) | Station Location | Soil pH[a] | MAT (°C)[b] | Average Annual Precipitation (L) | | |
|---|---|---|---|---|---|---|---|---|
| | | | | | | ECCC[c] | DAYMET[g] | This Work |
| Grand Codroy (GC) | 47°50'43.1"N 59°16'16.0"W | Stephenville A (8403801) | 48°32'29.00" N 58°33'00" W | 3 to 4 | 5.0[e] | 53.2 | 58.9 | 45.6 (+5.17) |
| Pynn's Brook (PB) | 49° 05' 13.20"N 57° 32' 27.60" W | South Brook Pasadena (8403693) | 49°01'00" N 57°37'00" W | 3 to 4 | 4.6[e] | 21.4 | 54.3 | 38.6[h] |
| Salmon River (SR) | 51°15'21.6"N 56°08'16.8"W | Plum Point (40KE88) | 51°04'00" N 56°53'00" W | 3 to 4 | 2.4[e] | 47.1 | 45.4 | 32.3 |
| Eagle River (ER) | 53°33'00.0"N 56°59'13.2"W | Cartwright A (8501100) | 53°42'30" N 57°02'06" W | 3 to 4 | 0[d] | -[f] | 56.3 | 25.8 |

[a]Soil pH for the organic and mineral soil horizons determined by addition of 400 µL of aqueous 0.5 M $CaCl_2$ to a 50:50 w/w slurry of dried soil in deionised water. **Note: the four remote NL-BELT sites are dominated by balsam fir trees underlain by humo-ferric podzol soil with pH ranging between 3.0 and 4.5.**
[b]Environment Canada: Canadian Climate Normals, 1981 to 2010, https://climate.weather.gc.ca/climate_normals/ (last accessed: 14 July 2023).
[c]At least 20 years of measurements.
[d]The World Meteorological Organization's "3 and 5 rule" (i.e., no more than 3 consecutive and no more than 5 total missing for either temperature or precipitation).
[e]Annual precipitation averages determined using ECCC daily precipitation reports.
[f]Large quantity of missing data for this location from January 2015 to December 2016 prevents any reliable estimate.
[g]Estimated deposition rates converted to volume using DAYMET (Thornton et al., 1997, 2021, 2022).
[h]Volumes merged for 2015 and 2016 at PB and HR.

### 2.3.1 Sample Preservation

Four of the six sample containers (two each of OF and TF) were biologically sterilized using 1 mL of a saturated aqueous solution of mercuric chloride ($HgCl_2$) to preserve against biological growth and loss of bioavailable nutrients over the collection periods. Unsterilized sample containers (without $HgCl_2$) were used for measurements of recalcitrant species and to assess any matrix effects exerted on target analyte quantitation. **The use of $HgCl_2$ as a sample preservation technique has been long-studied and well-established (Kirkwood, 1992; Kattner, 1999); thus, additional tests to verify the preservation of collected chemical species over time were not performed. The analysis of deposition collected in unsterilized and sterilized containers, however, serves as a method for internal sample validation - as does**

**our evaluation of measurement outcomes in comparison to those reported within the literature**. Collected sample volumes were measured with a 1000 ± 10 mL graduated cylinder and aliquots were collected for chemical analysis via transfer to precleaned 500- or 1000-mL HDPE containers (Nalgene; VWR International). Samples were stored at 4°C before returning to the laboratory where they were filtered with a 1000 mL Nalgene vacuum filtration system (P/N ZA-06730-53; ThermoFisher Scientific, Waltham, MA), fitted with 0.45 µm polyethersulfone filters (PES, P/N HPWP 04700, EMD Millipore), to remove suspended solids. Filtered samples were transferred to new clean HDPE containers and stored for up to two months at 4°C in a cold room until analysis. **The target analytes in this work are non-volatile and the described sample collection methods consider this analyte property, as well as their interactions with container materials. The versatility of the system design allows for the use of different collection materials, keeper solvents for volatile organics, etc., so that the experimental design can be analyte specific, depending on end user needs. Sample preservation approaches should thus be identified by users of this new platform based on their scientific objectives and review of the literature (Galloway and Likens, 1978; Peden et al., 1986; Dossett and Bowersox, 1999; Wetherbee et al., 2010). In addition to the internal validation approach described here, we aim to demonstrate that the precipitation samplers in this work are suitable for measuring conductive deposition on- and off-grid. Below we highlight autonomous off-grid operations, determine the fraction of conductive rainfall collected from the total volume of precipitation, and validate our measurements through comparison to the literature.**

### 2.4 Cleaning and Preparation of Sample Containers

All sample collection and storage containers, as well as all sample handling apparatuses, were made of HDPE or polypropylene for the quantitative analysis of target analytes. Prior to use in handling samples, these were all acid-washed in 10 % v/v HCl (P/N BDH7417-1; VWR International) followed by six sequential rinses with distilled water and ten rinses with 18.2 MΩ·cm deionised water (DIW; EMD Millipore Corporation, Billerica, MA, USA). Containers were dried by inversion on a clean benchtop protector overnight, or with protection from dust using lint-free lab wipes over container openings when necessary. Field and method blanks were collected through the addition of DIW to cleaned containers, and/or sample handling devices, in

order to quantify appropriate method detection limits and to identify any sources of systematic or random contamination. **Blank subtraction was applied to measurements, where appropriate.**

### 2.5 Measurements of pH and Conductivity

The pH and conductivity of each sample was determined using a ThermoScientific™ Orion Versa Star meter (ORIVSTAR52) interfaced with a pH electrode (Model: 8157BNUMD, Ultra pH/ATC Triode, ROSS) and 4-electrode conductivity cell (Model: 013005MD, DuraProbe, ROSS). Prior to use, the probes were calibrated daily with standard solutions specific for these probes (ThermoScientific™ Orion™ conductivity standard 1413, and pH 4, 7, and 10 buffers) and then stored between analyses according to manufacturer directions. Aliquots of 15 mL of precipitation from archived samples were subsampled into 40 mL polypropylene Falcon tubes. This was followed by immersion of a cleaned electrode for the conductivity measurement, followed by the pH probe measurement to prevent conductivity bias due to potassium chloride migration across the glass frit of the pH probe. Readings were recorded once signals had stabilized.

### 2.6 Measurements of Dissolved Organic Carbon (DOC)

Measurements of DOC were performed by catalytic combustion of samples in a platinum bead-packed quartz furnace at 720°C to quantitatively produce $CO_2$, followed by non-dispersive infrared absorption spectrophotometry using a Shimadzu Total Organic Carbon (model: TOC-V) analyzer and an autosampler (model: ASI-V). Cleaning of materials prior to DOC determination follows the same procedure as for the sample containers. Precipitation aliquots of at least 12 mL were transferred to clean and combusted (500°C, 5 hours) 40 mL borosilicate glass vials, then capped and stored at 4°C until analysis. Prior to analysis, vial caps were replaced with cleaned polytetrafluoroethylene-lined septa. Inorganic dissolved carbon (e.g., $H_2CO_3$) was purged from samples by acidification to pH 2 with HPLC grade $H_3PO_4$ (20 % v/v) and bubbling with an inert carrier gas. Samples were analyzed in triplicate and quantified using calibrations spanning 0.1 to 10 or 10 to 100 ppm (mg C $L^{-1}$) with potassium hydrogen phthalate (KHP), depending on the relative sample concentration range. Accuracy and precision were assessed using 1 and 10 ppm KHP check standards analyzed every 10 injections, respectively. Calibrations were performed at the beginning of every analysis day.

## 3.0 Results and Discussion

In addition to the general design advantages in the section that follows, we present the results of various physical and chemical parameters to validate this new open source custom-built modular system. The power consumption and snow-free performance testing are used to demonstrate the off-grid capabilities of these samplers, as are the two-year datasets. The lower power requirements are compared to existing commercial samplers and paired with solar top-up to prolong the use and reduce the need to replace batteries on timescales shorter than planned sampling duration (i.e., < 1 month). We then evaluate the automated wet deposition volumes, in which the samplers prevent dilution during atmospheric washout events, compared to total volumes collected from co-located samplers to depict the fractionation by volume as a function of time. We also investigate the advantages of replicates collected across the four watersheds, using deployments of triplicate samplers under field conditions. The ratio of collected TF to OF replicates highlights the ability of these samplers to capture the dynamic nature of precipitation interacting with forest canopies. Simple pH and conductivity measurements are then used as benchmarks to situate the NL-BELT data within the established literature to emphasize the robust operation of the samplers and impact of the selective sampling. Fluxes of DOC are also interrogated across all four sampling sites as we demonstrate the potential of these samplers to make measurements of more complex analyte pools that are of current interest to the atmospheric measurement community.

### 3.1 General Design Advantages

**While several precipitation collectors have been similarly developed to address specific scientific objectives – e.g., the quantitation of dust in wet and dry deposition (Laurent et al., 2015; Brahney et al., 2020), determination of ions and DOC in a tropical rainforest (Germer et al., 2007) and urban environments (Audoux et al., 2023), here we present a more general design for modular adaptability.** When compared to other precipitation collection apparatuses, the automated precipitation sampler developed in this work has several advantages. Most notable is the ability to collect integrated samples at remote locations by exploiting its off-grid capabilities. Our approach also maximizes the sensitivity of the rain sensor as long as electrolytes remain in the water reaching it. The chute ensures that even if the precipitation contains ultra-trace analyte quantities, they are still collected and quantified for an extended period when

high-purity water may be deposited during an atmospheric wash-out event. The chute does this by accumulating water-soluble materials between rain events that require time to be completely washed off and through the release of ions from the material itself, which ages under environmental conditions. As the conductivity of the precipitation falls below the sensor threshold **– conductive precipitation being that which initially contains high solute levels that progress through trace level concentrations**, the added ions from the chute prolong the collection of rain past this time point. In rainfall events where extended atmospheric wash-out occurs, **where precipitation becomes ultrapure water**, the sampler lids will eventually close – preventing dilution of the sample while maintaining the collection of analytes of interest. **A recent study has found that rainfall events could exhibit variability and the lower atmosphere can be supplied with aerosols due to specific sources, atmospheric dynamics, and meteorological conditions (Audoux et al., 2023). If this occurs, the automated lid will reopen to sample the polluted air masses.** In application to trace pollutants, this also reduces methodological sample preparation time as it decreases the extent to which additional handling steps, like solid-phase extraction, are required prior to analytical determinations.

The six replicate measurements used in each array provide a means of assessing sampling reproducibility (e.g., canopy TF has expected heterogeneity) and for multiple analyte classes to be targeted. Various analytes, with different chemical properties and/or contamination considerations, can be targeted by changing the materials used for the components that encounter the sample (i.e., lids, funnels, and sample holding containers). Replicate collection can also allow for selective sample preservation when quantifying deposited chemical species that may be reactive, volatile, or biologically transformed. The modularity of the overall system design also allows the collection units to be dismantled entirely and easily reassembled on-site, minimizing logistical issues and costs for transport to remote regions. Lastly, these collection units are cost-effective. We were able to produce four arrays, each consisting of six collection units, at a fraction of the cost of a single equivalent commercial off-grid automated precipitation sampling unit.

With the majority of commercial precipitation samplers requiring a source of electricity, on-grid sample collection necessitates high infrastructure costs and/or samplers being positioned closer than desired to point sources of anthropogenic pollution. As a result, especially in remote locations, site selection becomes heavily restricted and expensive when factoring in all the standard criteria, particularly with respect to the need for an easily accessible power source. Thus,

552 the off-grid capabilities of our samplers lend dexterity to these systems and makes deposition
553 sampling that follows standard siting guidelines, like those of CAPMoN or NADP but without
554 power, more accessible to the global atmospheric research community (Vet et al., 2014). To further
555 highlight and validate their capabilities, a series of fundamental performance parameters were
556 collected and are discussed in detail in the sections that follow.
557
558 **3.2 Power Consumption and Performance Testing**
559 **3.2.1 Power Consumption of Instrumental Setup**
560 The simplicity of the automated precipitation samplers allows for low power consumption
561 during operation, which is particularly important for off-grid operation. The motors operating and
562 rain sensor heating during active precipitation are the most energy-intensive elements of the system
563 (Table 2). The integrated contribution of the motor over a month-long sampling period is however
564 negligible compared to other components, since it is operational for short periods of 5 to 10
565 seconds with a current usage of only 38 mA. The continuous need to provide 5 VDC to the digital
566 logic via step-down from 12 VDC is actually the largest power consuming component of the setup
567 in the absence of rain. When the samplers are in the closed position, under rain-free conditions,
568 the power consumption of the entire array is 4.66 Watts (W) and 2.86 W for transformed 115 VAC
569 and battery 12 VDC supplies, respectively. The provision of 12 VDC to the board with a
570 transformer for the 115 VAC application results in greater total power requirements. These values
571 increase to 10.00 W and 5.04 W with the detection of a conductive liquid on the precipitation
572 sensor as it heats the sensor surface to capture the active period of the event. Based on the measured
573 power consumption, a fully charged 103 Ah AGM battery would provide at most 447 hours (or 18
574 days) in standby mode under rain free conditions and 294 hours (or 12 days) if the heated surface
575 of the sensor is in continuous use (Table 2). The lower range limit is unlikely since the sensor only
576 operates for the duration of a rain event, after which the battery is available for solar top-up again.
577 In the fieldwork conducted here, battery life was extended through the addition of 40 W solar
578 panels to the systems. The entire array was confirmed to be operational at the end of monthly (SR,
579 PB, and GC) and two month (ER) integrated sampling periods on an ongoing basis, prior to
580 exchange with a new fully charged battery, for two years.
581

**Table 2.** Measured voltage, current, and power consumption of the rain sensor and circuitry in both the idle and maximally operational state when connected to a 12 VDC battery or transformed 115 VAC. Total power demand was measured for wet and dry sensor scenarios.

| | Rain Sensor | | AC Outlet | | DC Battery | | Total AC Outlet | | Total DC Battery | |
|---|---|---|---|---|---|---|---|---|---|---|
| **Parameters** | **Idle** | **Active** | **Idle Board** | **Motors In-Use** | **Idle Board** | **Motors in-Use** | **Dry** | **Wet** | **Dry** | **Wet** |
| **Voltage (V)** | 12 DC | 12 DC | 114 AC | 110 AC | 12 DC | 12 DC | - | - | - | - |
| **Current (A)** | 0.008 | 0.120 | 0.040 | 0.078 | 0.230 | 0.300 | - | - | - | - |
| **Power (W)** | 0.10 | 1.44 | 4.56 | 8.58 | 2.76 | 3.60 | 4.66 | 10.00 | 2.86 | 5.04 |

In comparison to two commercial samplers used by national monitoring networks, the power requirements of our new samplers are substantially lower. The first commercial sampler we reviewed draws a maximum of 2 A, with a ceramic heater housed within the sampler case that draws 0.8 A constantly, resulting in an upper limit power demand of 230 W (at 115 VAC) and a lower limit of 92 W. The commercial sampler can be upgraded to utilize a thermostated space heater for winter operation, drawing an additional 4.2 A (480 W), resulting in a maximum power demand of about 800 W when using a 115 VAC power supply. A second commercial precipitation sampler reviewed is used by national monitoring networks and draws approximately 5 A, resulting in a power requirement of 575 W at 115 VAC. The commercial and standard precipitation samplers for deposition monitoring programs have much higher power requirements compared to those presented in this work. The commercial samplers utilize 80 to 100 times more power. With our lower power requirements, the new automated samplers prove to be advantageous in both on- and off-grid sampling yet are disadvantaged in being unable to collect snow in the winter.

### 3.2.2 Precipitation Sampler Performance Tests and Data Logging

In addition to low power consumption during precipitation sampling, a supplied battery can obtain constant power renewal when outfitted with a solar top-up that is kept exposed to sunlight by proper orientation. At NL-BELT, adjustments were made for this during each site visit during sample collection. During the solar top-up tests below, voltages of the sensor and batteries were consistently monitored. Over a test period of 22 days, no appreciable decline in battery performance of a 76 Ah unit was observed despite the detection of more than 10 rain events during that period (Figure 3a).

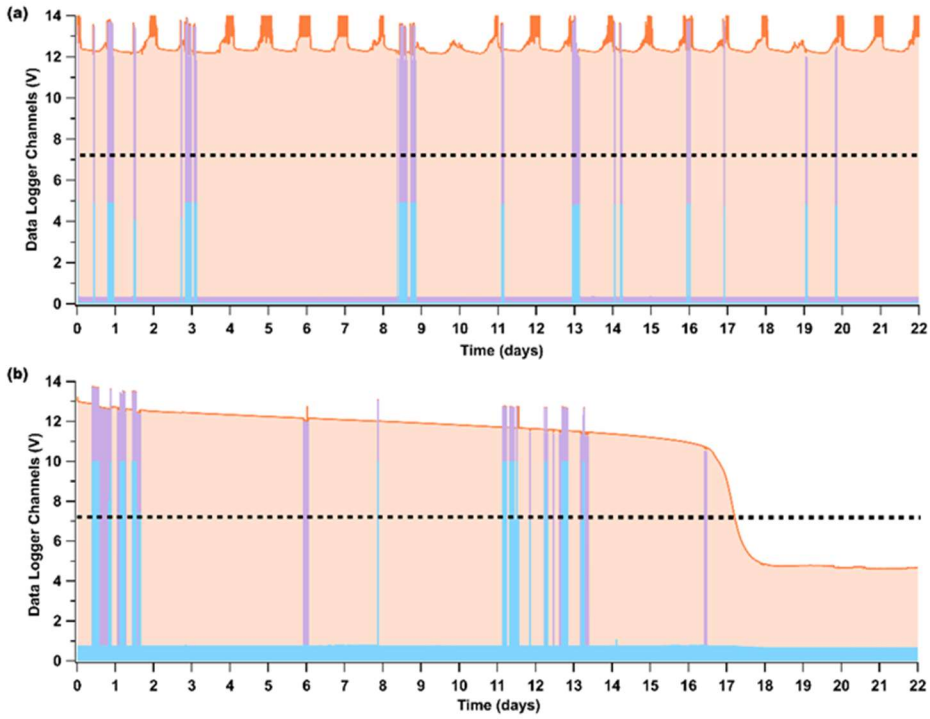


**Figure 3.** Performance of off-grid precipitation samplers during sample collections from **(a)** 13 July to 7 August 2018, using a 76 Ah battery and solar panel top-up and **(b)** 22 January to 13 February 2019 with a 103 Ah battery and no solar panel. Battery voltage (shaded orange) is elevated above 12 VDC when charging, or decreases over time when no solar panel is used and precipitation is sensed/collected. The 12 VDC rain sensor relay signal (purple) and the open sampling lid switch voltage (blue) indicate active periods of detected precipitation. The black dashed line indicates the 60% efficiency cut off, 7.2 V, at which the battery should be recharged.

In comparison, winter sampling with these devices is not recommended without substantial investment in a sufficient power density provided high-performance cold weather batteries. The lack of sunlight during winter at higher latitudes also negates the use of effective small scale solar top-up. Our tests show that when the samplers were deployed without a solar backup under snow-free winter conditions (temperatures ranging from -17.8 to 7°C), with a 103 Ah battery, the off-grid system only lasted for 17 days. At this point, the larger capacity battery was fully depleted by frequent snow and rainfall – probably due to the heated precipitation sensor requiring additional energy to phase change snow and ice to water and then to evaporate that water. This depletion occurred despite housing the battery in an insulated enclosure during the test. In addition, on days 6 and 16, the precipitation sensor relay was activated but the lid did not rotate to the open position (Figure 3b, blue trace). This could have been because the precipitation event was not intense

enough for the lid to open fully and trigger the 5 V lid open switch or because of snow and ice buildup around the lids resulting in them being unable to physically open. Overall, these samplers may be possible to deploy during the winter if line power can be supplied. Such a deployment would further necessitate that the sampling funnel be heated to render a liquid sample for collection in the jugs in addition to the sensor chute to prevent snow and ice accumulation. A heated funnel would also prevent snow or ice accumulation on top of the automated lids. Together, such power-hungry requirements for winter operation exceed simple off-grid use with a battery package that is easily transported into and out of remote field sites.

### 3.3 Comparison of Sample Collection Volumes

The automated samplers were colocated with total deposition samplers and deployed across the experimental forests of four NL-BELT regions during the 2015 and 2016 growing seasons to observe deposition trends. In addition, we compare these observations to the long-term climate normals reported by ECCC and estimated deposition at 1 km x 1 km resolution from the DAYMET reanalysis model (Table 1, **Section S2**). Three automated samplers were deployed in the open to collect incident precipitation (OF) and another three under the experimental forest site canopy (TF). The mean OF volumes of triplicate measurements from south to north were 1.42, 1.38, 1.31, and 0.79 L, whereas the corresponding TF volumes were generally similar in magnitude at 0.96, 0.98, 1.02, and 1.13 L, for the 2015-16 sampling period (Figure 4). It is evident that the volume of precipitation decreased as latitude increased for OF samples, whereas the opposite relationship was observed in TF samplers, although the absolute volumes are more comparable in magnitude. The total deposition volumes collected were as expected, decreasing from south to north in agreement with the expectations from the long-term normals and comparable to the estimates from the DAYMET model (Table 1), where the largest integrated volume of precipitation was collected at the lowest latitude (GC) and a lower amount at the highest latitude (ER), with the intermediate sites (HR and PB) having the lowest inputs overall during this observation period. Total annual deposition volumes collected by our deployed samplers from south to north in 2015 were 39.5, 39.4, 31.9, and 17.5 L, while in 2016 they were 51.7, 37.8, 32.8, and 34.2 L. Total deposition volume collected from HR was used for comparison to automated sample volumes collected at PB in 2015, as they both share the same watershed. This approach had to be taken, as the HR site was initially planned for full experimental use before becoming inaccessible in early 2015. The relative

error between the two sites for samples collected in 2016 was ± 15% (24.6 L in PB and 32.2 L in HR), comparable to the reproducibility we observe for replicates collected within a given site (see below). The total deposition samplers were installed in HR in late 2014 and the automated samplers were then set up at PB. Despite this, there is good agreement between the trends in predicted deposition values by DAYMET with the measured values, although the absolute amounts from these are systematically lower in all of our observations **(Section S2)**. Regardless, by following the recommended siting criteria from the NADP and CAPMoN as best as possible, the very strong agreement of our temporal trends at both annual and monthly timescales with both comparators demonstrates the suitability of the total deposition samplers and, therefore, the automated samplers for use in quantifying deposited chemical species of atmospheric interest into the experimental sites.

The wet deposition volumes collected for the snow free period using the automated precipitation samplers did not follow the trends in total deposition (Figure 4), as might be expected **(e.g., due to pollutant loading, rainfall quantity/rate, and scavenging processes).** For the 2015 collection period from June through October, the summed volumes of OF precipitation, from south to north across the NL-BELT, were 25.4, 10.9, 20.4, and 2.2 L, while in 2016 they were 17.3, 30.4, 13.5, and 5.1 L. **While the total and OF fractions would typically be much closer to unity in more polluted regions, it would be expected in these remote NL-BELT field sites for the differences to be driven by complex, non-linear processes that cannot be easily disentangled. Here we present** three reasons as to why the measured wet **OF** deposition volumes do not follow the total deposition trend across the transect. First, these samplers are designed specifically to collect only conductive precipitation (i.e., containing conductive atmospheric compounds) not total/bulk precipitation. As a result, the OF wet deposition volume collected across the sites is mostly below 50% of total volumes collected, while TF volumes are similar in magnitude or lower than that of OF (Figure 4). The wet deposition fraction collected was variable within and between regions, sometimes less than 10%, despite large volumes collected in total and presumably due to intense atmospheric washout that this region is well-known for. Second, the NL-BELT total deposition trend estimated using the ECCC long-term climate normals represents a 30-year period (Bowering et al., 2022) while the automated volume measurements here represent two years of targeted conductive precipitation collection. The combined summed volumes of targeted conductive wet deposition across the 2015 and 2016 field seasons were 42.7, 41.3, 33.9, and 7.3

L, somewhat better reflect the expected precipitation trends within the transect (Table 1). Lastly, our monthly automated wet deposition sample collection periods occurred from June through November and so it is temporally incomplete with respect to the substantial amount of precipitation volume deposited as snow delivered during the winter (Table S3). The discrepancies between the long-term trends and our shorter-term observations therefore make sense as they are sensitive to interannual changes in synoptic scale transport and rainwater solute loadings, as exemplified by the volumes collected in SR in 2015 (Figure 4b) and PB in 2016 (Figure 4c). Overall, for the automated sampler observations on a per-year basis, there is no consistent trend between site latitude and the volume collected in either OF or TF. This is unsurprising as they are dependent on the conditions that drive the rate of atmospheric wash-out and presence of conductive solutes.

The automated OF wet deposition volumes collected each year have peak values that range from 1 to 4 L with an overall variability of ± 33% for any triplicate of samples across the entire dataset. Across our 33 sample collection periods, our replicate relative standard deviations (RSDs) follow a log-normal distribution where volume reproducibility is typically within ± 12.5% and almost always within ± 31.5% (Figure S11). A few outliers with higher variability skew the overall view of volume precision. Out of 33 OF samples collected, **10** have RSDs greater than 40.5% with 2 of those **10** having RSDs greater than 100%. **Those values greater than 40.5% had no systematic relationship with site or time of time. Wind speeds were considered as a possible source of variability. The prevailing winds over Atlantic Canada are known to be southwesterly in the summer – intensifying during the autumn months – and westerly to northwesterly in the winter (Bowyer, 1995; Jacob, 1999; Randall, 2015). Strong wind speeds (i.e., >100 km/hr) could occur on an event basis during any time of the yes and, thus, could contribute to the variability seen at each field site.** Wind is known to generate bias in gauge-based precipitation measurements where unshielded precipitation gauges can catch less than half of the amount of a shielded gauge (Colli et al., 2016). A windscreen design for obtaining rainfall rates – and thus, volumes – to be more reproducible could be considered in future deployments of our developed samplers, similar to recently reported innovations for smaller rainfall rate devices (Kochendorfer et al., 2023). This would, however, increase costs and logistical considerations in deploying the developed devices which currently operate synonymously to deposition systems employed by government monitoring programs. **Our siting approach is consistent with these, which often deploy a single sampler without wind protection, Thus, by employing replicates,**

**we are able to ascertain the environmental variability.** In addition, collection of replicate samples allows our observations to span a wider physical area, reducing the impact of confounding variables such as wind speed in comparison to a more typical sample size of one for many field collections. Imperfect siting and lack of shielding is necessary where remote field sampling prevents the setup of such infrastructure. As a result, the deployment of triplicate samplers provides researchers with a better opportunity to implement quality control as they can reduce bias in the event of dynamic OF. While the effect of wind is reduced, additional factors can drive variability when the samplers are placed under a forest canopy for TF collection.

To demonstrate canopy dynamics impacting interception volumes within the sampling sites, the ratio of throughfall to open fall (TF/OF) volume was compared amongst our total pool of 31 samples. This group of samples encompassed the monthly average TF/OF values for each set of triplicate samplers, at all four sites, from 2015 to 2016. These measurements were then split into two separate populations – samples that have a TF/OF less than one (n=24) and those that have a TF/OF greater than one (n=7). The samplers were positioned identically between years and no single sampler was reproducibly found in the second population. In the first population, the fraction collected was 56 ± 21% (ranging from 19 to 88%), likely due to the known processes of canopy and stem interception (Eaton et al., 1973; Howard et al., 2022). For example, in two young balsam fir-white birch mixed forest stands, the amount of precipitation intercepted by the forest canopy, in similar snow-free conditions, was estimated to be 11 ± 5% (Hadiwijaya et al., 2021). In mature boreal forests, 9% to 55% of rainfall can be intercepted by the canopy (Pomeroy et al., 1999). Relevant to deposition of atmospheric constituents, Pomeroy et al. (1999) also reported that up to 70% of intercepted rainfall may evaporate directly from the canopy, which can leave behind non-volatile rainfall solutes. Wet deposition that undergoes stemflow (SF) proceeds down the branches, stems, and/or trunks of a plant, transferring precipitation and nutrients from the canopy to the soil at the trunk or stem base (Ciruzzi and Loheide, 2021). These known mechanisms of canopy interception ultimately reduce the amount of precipitation reaching the ground as TF, and thus, this explains the smaller volumes found in our samplers compared to the OF measured simultaneously. In contrast, the fractions that ranged from 108% to 424%, averaging 186%, demonstrates a different aspect of the highly dynamic nature of canopies where they can sometimes intercept rainfall like an impermeable surface to act as a funnel, guiding large volumes of precipitation on to the ground, or in this case into the TF samplers (Metzger et al., 2019).

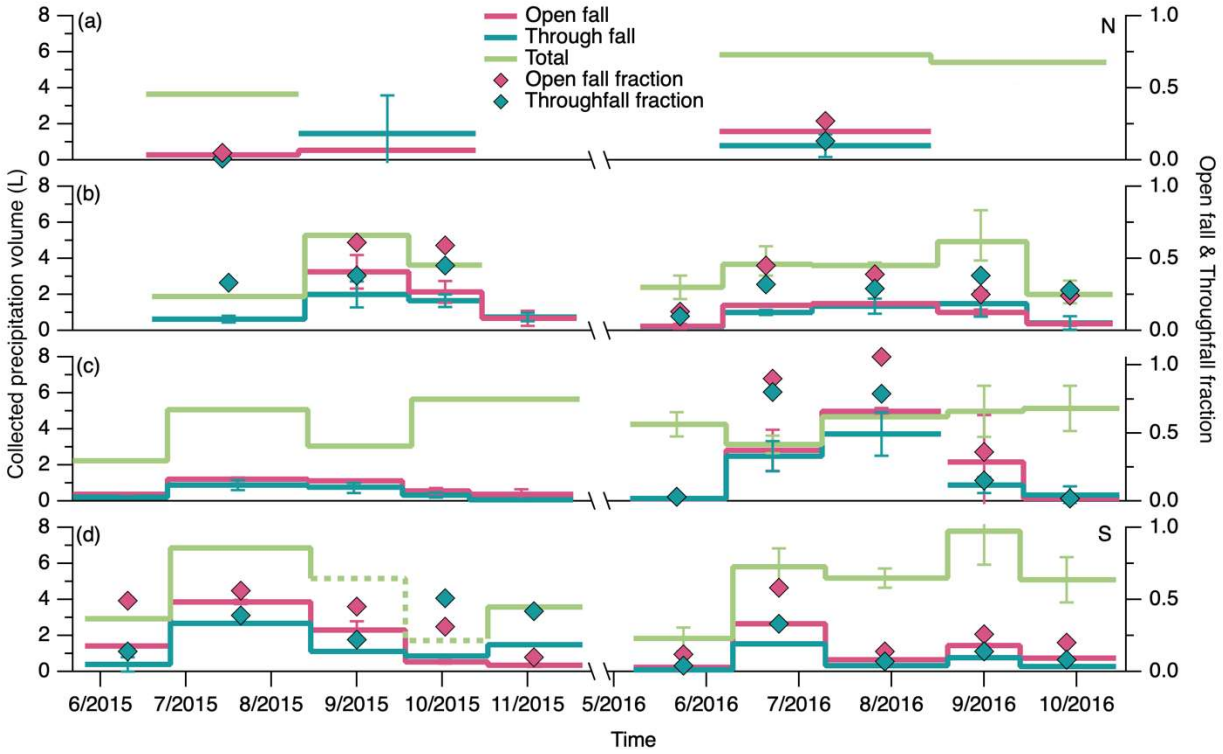


**Figure 4.** Average volume collected from replicate automated samplers deployed from June 2015 to October 2016, from north (N) to south (S), at the NL-BELT field sites: **(a)** ER, **(b)** SR, **(c)** PB, and **(d)** GC. The red trace represents open fall, teal for throughfall, and light green for total deposition (the sum of conductive and non-conductive precipitation). The total precipitation volumes depicted for PB, from July 2015 to November 2015, were collected at the nearby HR site in the same watershed since no total deposition measurements were in place at PB during this period. The missing volume for GC in 2015 was estimated from the determined ECCC station linear relationship and is presented as a broken line. The fraction of precipitation collected as open fall or throughfall, compared to the total deposition (right axis), are represented by diamonds of the corresponding color. Error bars represent the standard deviation of three measurements from replicate samples. The axis break spans the winter months when the off-grid automated samplers were stored.

### 3.4 Characterizing Chemical Parameters from NL-BELT

In addition to assessing physical parameters, chemical parameters were also evaluated in this work. Conductivity and pH are measurements commonly made on precipitation samples collected from the field and so incorporating them into our analysis is useful for instrumental validation. Additionally, with increasing recognition of their importance as a proxy for ROC estimation, and in biogeochemical carbon budget closure, DOC flux measurements were used to compare against a limited number of prior reports, each using different sampling or data interpretation strategies. These chemical measurements were also made in an underrepresented

part of the world in terms of atmospheric deposition sampling and are useful additions to the overarching study of precipitation chemistry.

### 3.4.1 Precipitation pH

The deposition of atmospherically persistent pollutants and biogeochemically relevant species to the Earth's surface, or even $NO_3^-$ and $SO_4^{2-}$ historically, can affect the environmental health of soil, air, and water. With the pH range of natural rainwater in equilibrium with atmospheric $CO_2$ expected to be between 5.0 to 5.6, acid rain is defined by values lower than this (Han et al., 2019). Traditionally, the extent of acidity depended on the intercepted atmospheric concentrations of $HNO_3$ and $H_2SO_4$. In any case, monitoring acidity and deposition is especially relevant in remote regions, where major uncertainties and gaps in deposition measurements and global ion concentrations exist (Escarré et al., 1999; Vet et al., 2014). A change in pH can modify the chemical state of many pollutants, altering their transport, bioavailability, and solubility (Guinotte and Fabry, 2008). For example, this can increase exposure and toxicity of metals and nutrients in marine habitats which can go undetected for longer periods in remote areas.

Most TF samples were observed to have slightly higher pH than those from OF which had pH values ranging from 4.14 to 5.71 (Figure 5, Table 1). The TF precipitation pH, on average, ranged from 4.74 to 5.99 with rare exceptions falling outside of that range (e.g., July and September 2015 PB pH of 3.69 and 4.26, respectively, and the July 2015 GC with pH of 4.12). Excluding these exceptions, there are no major variations observed spatially between the four sites, or temporally between seasons or years (Figure 5). The pH values reported at each of the NL-BELT field sites are comparable to recent OF measurements made at CAPMoN sites in Nova Scotia and Newfoundland and Labrador, where the reported pH of precipitation ranged from 4.44 to 5.19 (Houle et al., 2022). The more basic TF overall is expected, as it has been found that up to 90% of $H_3O^+$ in precipitation can be absorbed by leaves while passing through the canopy (Cappellato et al., 1993). Foliar leaching, the release of ions from leaves, has been commonly reported for base cations such as $Mg^{2+}$, $K^+$, and $Ca^{2+}$ while being minimally observed for other ions such as $Cl^-$ and $SO_4^{2-}$ (Carlson et al., 2003). Mechanisms for foliar leaching include passive cation exchange of $H_3O^+$ with, for example, cells in the interior of the leaf (Burkhardt and Drechsel, 1997). Additionally, alkaline dust – deposited on the leaves of the canopy, can decrease the acidity of TF precipitation. Such dust can accumulate on leaf surfaces as a result of anthropogenic (i.e., industrial

processes) or natural (i.e., wind erosion) sources (Csavina et al., 2012), so that precipitation passing through the canopy can interact with it (e.g., $CaCO_3$); thus, neutralizing acidic species and increasing the TF pH observed in our automated samplers.

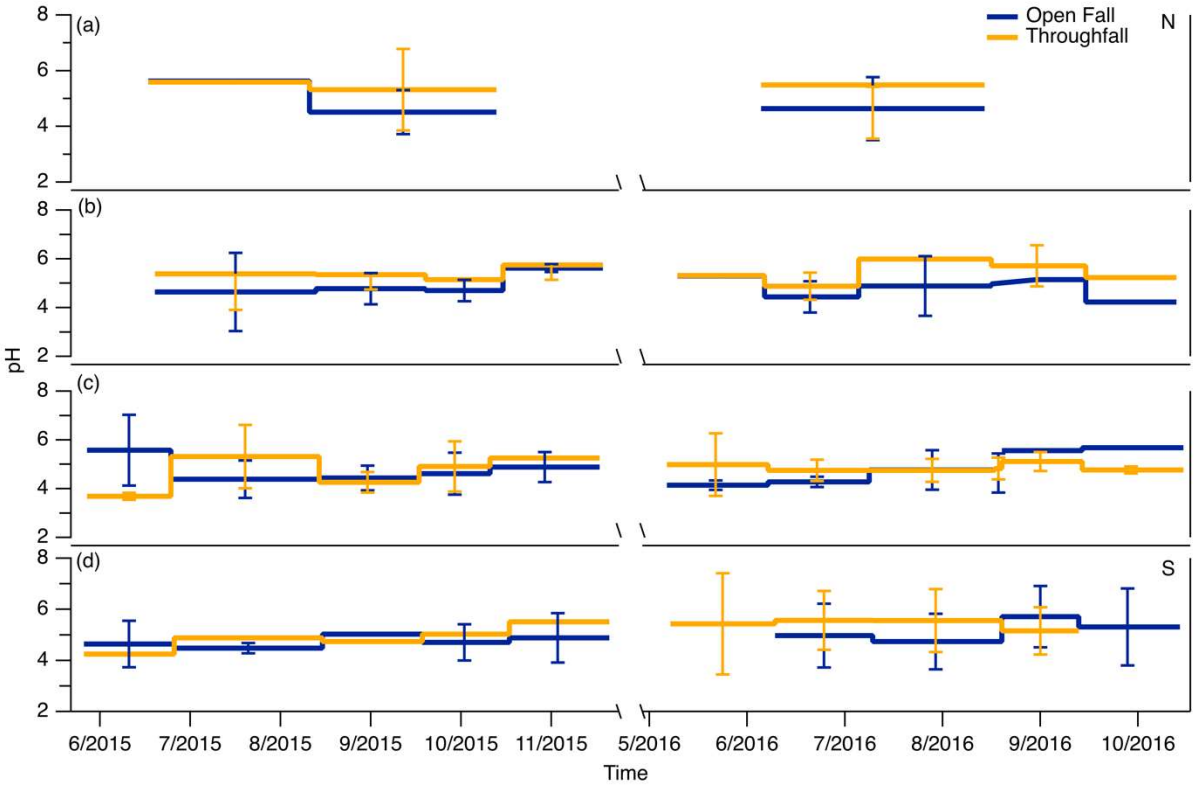


**Figure 5.** Average pH values from replicate samples collected at each NL-BELT field site, from north (N) to south (S), at **(a)** ER, **(b)** SR, **(c)** PB, and **(d)** GC, from June 2015 to August 2016. Open fall collections are represented using the solid blue trace whereas the orange trace is the pH of the precipitation collected as throughfall under the balsam fir canopy.

The pH of the collected precipitation appears to be similar in both TF and OF as a function of time – despite the potential for foliar leaching and dust dissolution in the canopy. The same chemical components may be setting the pH, as these measurements do not vary much seasonally, geographically, or temporally. As pH is a long-studied measurement, its purpose in this work was to validate the sample quality from our described collection approach, rather than drive any scientific objective. Nevertheless, while the NL-BELT measurements demonstrate a recovery compared to rainwater pH in 1980s eastern North America – prior to $NO_x$ and $SO_2$ regulation (pH from 4.1 to 5.0; Barrie and Hales, 1984), the present-day pH remains lower than expected for natural rainwater (~5.6; Boyd, 2020). Keeping in mind the successful environmental policies limiting $SO_2$ and $NO_x$, leading to considerable decreases in atmospheric concentrations of $H_2SO_4$

and $HNO_3$, a modern view on the trajectory of continental U.S. cloud water composition and pH has recently been reported (Lawrence et al., 2023). Across the U.S. and eastern Canada, measurements of anion molar charge equivalents have been lower than cations – a potential explanation being an increase in the presence of weak organic acids which commonly have pKa values near 4 (Feng et al., 2021), an outcome we have also observed in aerosol sample chemical composition from Atlantic Canada (Di Lorenzo et al., 2018). With the frequency of acid rain having a pH < 5 decreasing over the past 20 years, these recently reported measurements depict deposition composition shifting away from a 'linear' chemical regime dominated by $H_3O^+$ and $SO_4^{2-}$ towards a 'non-linear' regime designated by low acidity, moderate to high conductivity, potentially weak acid-base buffer systems, and increasing base cation and TOC concentrations (Lawrence et al., 2023). It would seem the evolving chemical contributors to global rainwater pH remain an open line of investigation.

### 3.4.2 Precipitation Conductivity

In all the collected OF and TF precipitation samples, across all four NL-BELT sites, the average measured conductivity values ranged from 21 to 166 µS/cm **following no apparent seasonal or temporal trend** (Figure 6). **Additionally, the conductivity in both OF and TF also appear to vary across the field sites - only within the 2016 TF samples does the conductivity appear to increase with decreasing latitude.** Yet, with the typical conductivity of surface and drinking waters being between 1 to 1000 µS/cm (Lin et al., 2017), and typically below 200 µS/cm in stream water measurements within the watersheds of each of the NL-BELT sites, our observations are comparable and fall within the expected range. Our field blanks – encompassing a variety of materials and apparatuses, and our cleaning procedures, routinely produced conductivities of 9 ± 5 µS/cm. The conductivity of saturated $HgCl_2$ in water (at 0.1% vol/vol) was 13.6 ± 0.4 µS/cm, which is also comparable to **but statistically higher than** our field blanks **(p = 0.0015; unpaired t test)** and less than what was observed for our samples **($p < 2 \times 10^{-6}$ for each site considered separately and also across all sites; unpaired t-test).** Even with this background correction applied, the conductivity values presented here are expected to be similar to or higher than what would typically be found in rainwater (4 to 150 µS/cm; Beverland et al., 1997) as the rain sensor deliberately selects for precipitation containing ionic chemical components with conductivity greater than 1.0 µS/cm, while excluding pure water during atmospheric washout,

858 which would dilute the dissolved solutes in the wet deposition sample and lower the resulting
859 conductivity values. The overall comparability between our range and those previously reported,
860 where the lower limit is slightly higher in our dataset, demonstrates that the principle of operation
861 of our instrument is robust. It decisively collects precipitation with the property of conductance
862 indicating dissolved ionic solutes of interest to atmospheric chemical processes.
863

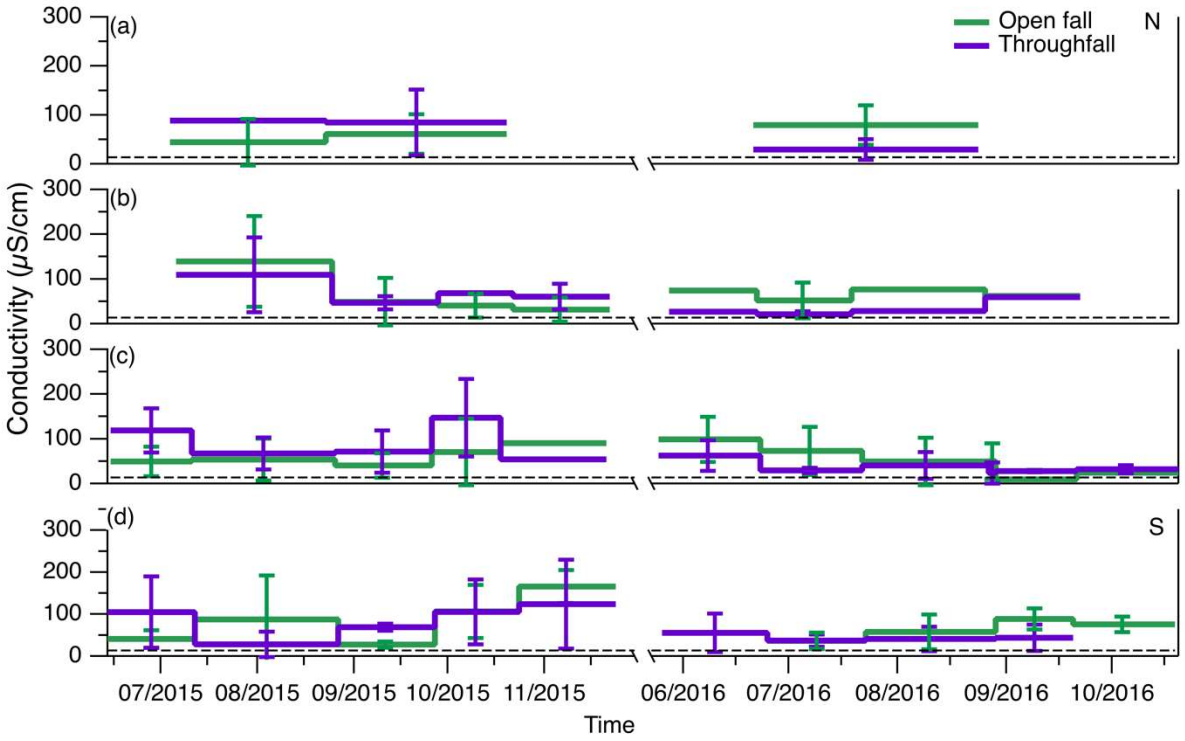


864
865 **Figure 6.** Average conductivity measured from replicate automated samplers at the NL-BELT
866 field sites, from north (N) to south (S), at **(a)** ER, **(b)** SR, **(c)** PB, and **(d)** GC, from June 2015 to
867 October 2016. The green trace represents open fall samplers whereas the purple trace represents
868 throughfall samples. The error bar represents the standard deviation between replicate
869 measurements. The dashed black line represents the upper threshold of conductivity (13.6 µS/cm)
870 that arises due when an addition of saturated aqueous $HgCl_2$ is made to microbially sterilize
871 samples. Note that all samples have conductivities equivalent to or higher than 13.6 µS/cm.
872
873 **3.4.3. Wet Deposition of Dissolved Organic Carbon (DOC) at NL-BELT**

874 The concentration of DOC in OF and TF precipitation, across all four sites, ranged from 3
875 to 46 mg $L^{-1}$ and 5 to 65 mg $L^{-1}$ with averages of 16 ± 10 mg $L^{-1}$ and 22 ± 12 mg $L^{-1}$, respectively
876 (Table 3). Concentrations are influenced by the volume collected and are not useful when
877 discerning deposition trends and/or mechanisms. The concentrations were converted to elemental
878 fluxes using the volume of precipitation collected, the area of the funnel and the number of

879 sampling days of each sampling period (Figure 7). The total flux for each sample period was
880 summed **and reported as an equivalent annual flux with the following units: mg $m^{-2}$ $a^{-1}$.**
881 **Annual fluxes** ranged from 600 to 4200 mg C $m^{-2}$ $a^{-1}$ across the study sites for the snow free period
882 (Table S4).
883 The TF DOC fluxes were enhanced compared to the corresponding OF samples as
884 precipitation was intercepted by the forest canopy, with fluxes higher in TF samples by 600, 400,
885 and 400 mg C $m^{-2}$ $a^{-1}$ at GC, SR, and ER, respectively (Table S5). The accumulation of water-
886 soluble organics on forest canopies that increases DOC detected in TF could originate in part from
887 organic carbon-containing compounds aged through oxidation reactions in the atmosphere, which
888 increases their water solubility and propensity for surface interactions. In periods without
889 substantial rain, these oxidized organics deposit effectively to the high surface area of forest
890 canopies, contributing to the elevated DOC measured in TF. Additionally, non-volatile organics
891 left behind from evaporated precipitation intercepted by the canopy could also contribute.
892 Conversely, other mechanisms within the forest could result in enhanced DOC in TF. Recently,
893 Cha et al. (2023) utilized a mass balance approach to determine whether DOC deposition is driven
894 by canopy leaching (i.e., soluble tree resin, leaf exudates, internal tissues and microbes) or
895 dissolution of dry deposited gases and $PM_{2.5}$ on plant foliage into rainwater. It was found that
896 canopy leaching is the major contributor to TF DOC, accounting for ~83% of throughfall DOC.
897 Whereas, $PM_{2.5}$ and rainwater only accounted for ~3 and 14%, respectively, while dry deposited
898 gases were not considered. This suggests that internal cycling of DOC within the forest could be
899 an important source of DOC to the throughfall soil interface (Cha et al., 2023). It is possible that a
900 similar mechanism may be responsible for the elevated levels of DOC in TF at the NL-BELT sites,
901 but we cannot explicitly distinguish between internal cycling versus external deposition in the
902 current study.
903 A notable exception was observed at PB, where the DOC fluxes in the open fall sample
904 were enhanced up to 1800 mg C $m^{-2}$ $a^{-1}$ when compared to the TF in 2016. This may be attributed
905 to a difference in forest type within this NL-BELT region being black spruce (*Picea mariana*)
906 instead of balsm fir (Bowering et al., 2023). Some studies have suggested that forest type could be
907 a major factor affecting DOC variability (Arisci et al., 2012; Sleutel et al., 2009). Specific
908 differences in canopy height, leaf area index, canopy structure and the shape of leaves and needles
909 could drive DOC differences between forest types (Smith, 1981; Erisman and Draaijers, 2003;

910 Sleutel et al., 2009). The elevated levels in OF samples relative to TF within PB are consistent
911 with idea of uptake and/or leaching of canopy DOC in the internal cycling of DOC, while the
912 enhanced TF at the rest of the sites is more difficult to observational constrain the participating
913 processes.

914 Episodic events, such as polluted air masses from wildfires could also result in elevated
915 deposition of DOC. It is estimated that ~116 – 385 Tg C $a^{-1}$ is produced globally due to the
916 incomplete combustion of biomass during landscape fires (Santín et al., 2016; Coward et al., 2022).
917 Several studies have associated enhanced DOC levels with wildfires (Gao et al., 2003; Moore,
918 2003; Wonaschütz et al., 2011; Myers-Pigg et al., 2015). More recently, Coward et al. (2022)
919 measured DOC in Pacific surface waters along the California coastline and observed 100 to 400
920 % increases in DOC concentration, when compared to pre-wildfire conditions. It is possible that a
921 similar biomass burning plume that underwent atmospheric washout, could be responsible for the
922 enhancement in the observed DOC at NL-BELT, overlaid on a background more typical of
923 seasonal oxidation of biogenic DOC. This also coincides with the seasonal variability observed in
924 OF samples from the same summer where elevated levels of DOC were measured. For instance,
925 the DOC deposition at PB for August 2016 was 4800 mg C $m^{-2}$, whereas the total deposition for
926 the same year was 7800 mg C $m^{-2}$ $a^{-1}$. This single period accounts for 62% of the total DOC
927 deposition at this site. This underscores the pivotal role that episodic transport may play in
928 influencing the dynamics of DOC deposition, particularly with a warming future where wildfires
929 are more prevalent.

930 The deposition trend observed in the current study also highlights the complexity of the
931 varied drivers of atmospheric ROC, in which some months have more DOC in TF versus OF and
932 occasionally the opposite is observed. Generally, we observed similar fluxes in both samples –
933 suggesting that the amount of deposited carbon is comparable. Although the volume of
934 precipitation captured in TF samplers are generally lower when compared to the corresponding
935 OF samplers, the deposition flux of DOC is greater in TF samplers. With DOC enhanced in TF
936 samples, the values reported here could be an underestimation of the amount of carbon reaching
937 the forest floor during precipitation events due to competing processes within the canopy. One
938 such process is stemflow (SF), where a fraction of precipitation intercepted by the forest canopy
939 is funneled over the bark of the tree surface to the base of the tree stem (Oka et al., 2021). Although,
940 SF was not measured in the current study, several studies have demonstrated that DOC

concentrations are enhanced in SF when compared to the corresponding TF and bulk precipitation samples (Stubbins et al., 2017; Van Stan and Stubbins, 2018; Ryan et al., 2021). Additionally, we cannot rule out that the chemical speciation differs between OF, TF, and SF even if the DOC values are similar, but such insights require more selective instrumentation for chemical analysis (e.g., high resolution mass spectrometry).

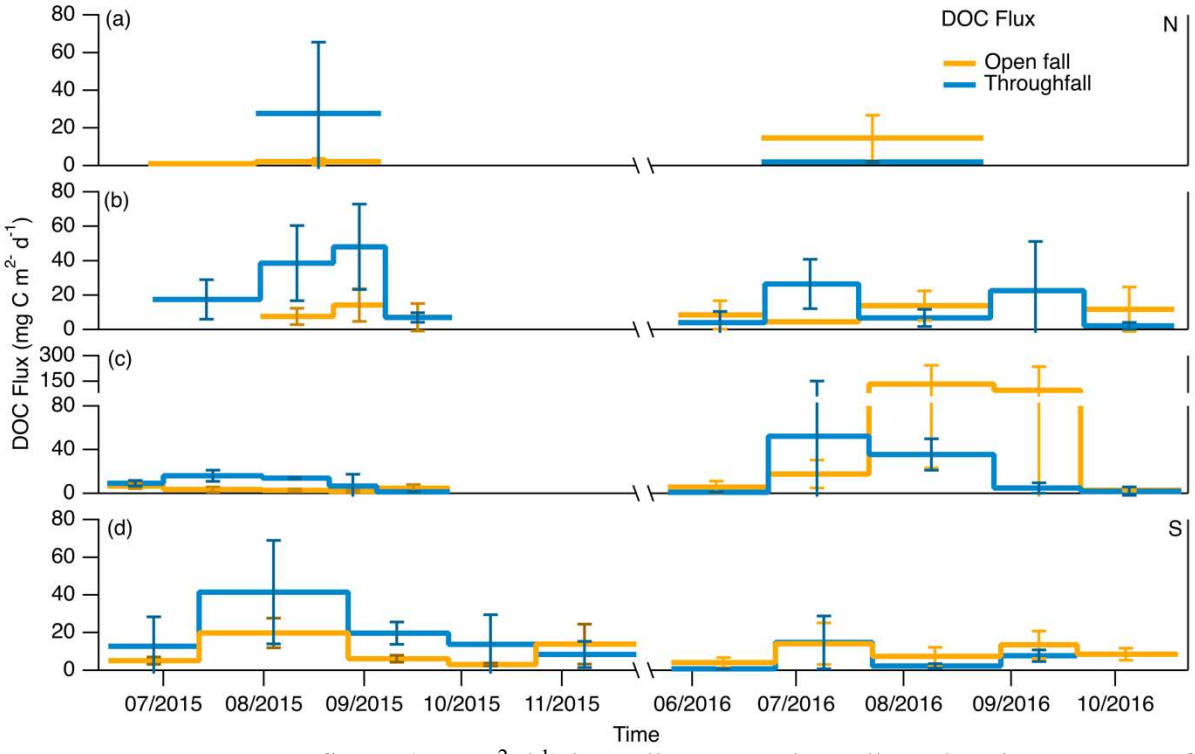


**Figure 7.** Average DOC fluxes (mg $m^{-2}$ $d^{-1}$) in replicate samples collected at the NL-BELT field sites, from north (N) to south (S), at **(a)** ER, **(b)** SR, **(c)** PB, and **(d)** GC, from June 2015 to August 2016. The yellow trace represents samplers that were placed in the open without any obstruction whereas the blue trace represents samplers that were placed under the canopy. Error bars represent the standard deviation of three measurements from three independent samples.

**The ability to accurately determine DOC in OF and TF precipitation demonstrates the capability of the automated deposition samplers. To validate our measurements, we compared our observed fluxes to other studies in different forest types.** Mean annual DOC fluxes were generally similar to those reported in some other boreal forests (Table 3). These include Finland, with work in stands that consisted mainly of Scots pine (*Pinus sylvestris L.*) (mean OF 2.32; TF, 4.35 g C $m^{-2}$ $a^{-1}$; Pumpanen et al., 2014), as well as in Mont St. Hilarie, Québec (mean OF 0.49; TF 2.05 g C $m^{-2}$ $a^{-1}$; Dalva and Moore, 1991), which also consisted of a variety of tree

962 species such as yellow birch (*Betula allenghanien*), red maple (*Acer rubrum*), and sugar maple
963 (*Acer saccharum*). Conversely, the annual fluxes were orders of magnitude lower than
964 measurements made at the University of Georgia (23 to 48 g C $m^{-2}$ $a^{-1}$) which has a subtropic
965 climate consisting mainly of southern live oak (*Quercus virginiana Mill.)* and eastern red cedar
966 *(Juniperus virginiana L.)* occasionally hosting dense epiphytes (Van Stan et al., 2017). This
967 highlights the potential variability to expect when measuring DOC in different forest systems, as
968 the annual DOC fluxes vary depending on factors such as climate, tree species composition, and
969 environmental conditions.

970 These results underscore the pivotal role the off-grid custom-built automated deposition
971 samplers can play in advancing scientific research, particularly in precipitation monitoring and
972 analysis. The automated system enabled long term continuous sample collection in remote
973 locations, which was previously challenging to attain due to the need for frequent human
974 intervention and resources required to regularly access these experimental forest stands. These
975 samplers also allowed us to compare DOC through replicate measurements in TF and OF samples
976 which sheds light on the potentially different DOC deposition chemistries within the NL-BELT
977 region. The automated system better maintains the integrity of DOC in the samples. **This was**
978 **achieved by following standard procedures for biogeochemical sample preservation (i.e.,**
979 **adding $HgCl_2$) (Argentino et al., 2023), employing a rigorous cleaning procedure, and**
980 **preventative design against the intrusion of forest litter** which could result in a positive bias
981 for DOC in the collected precipitation. The use of replicates also results in more robust scientific
982 conclusions and broader applicability of the results, and they can be obtained for a fraction of the
983 cost of a commercial equivalent, highlighting the contribution these automated systems are capable
984 of when applied to current precipitation monitoring. As a result, these samplers show promise in
985 the quantification of biogeochemical and anthropogenic chemical species of interest, which will
986 be visited in future manuscripts drawing from the samples presented in this dataset, and others
987 since obtained, but are beyond the scope of this manuscript in demonstrating the performance of
988 this new instrumentation.
989
990 **Table 3.** Concentrations (mg C $L^{-1}$) and annual fluxes (g C $m^{-2}$ $a^{-1}$) of DOC in precipitation (P),
991 open fall (OF), throughfall (TF), and stemflow (SF) collected at forested sites. Where volumes are
992 not available for other studies, fluxes are not possible to calculate. The values reported in the
993 current study are the estimated DOC flux for the wed deposition sampling period (~June through

October) for each year and therefore represents the lower limit of DOC deposition, as the dataset excludes snow.

| Site | Type | Mean Concentration (mg C $L^{-1}$) | Annual Flux (g C $m^{-2}$ $a^{-1}$) | References |
|---|---|---|---|---|
| Grand Codroy, NL, Canada (2015 to 2016) | OF | 12.83 | 1.56 | This study |
| | TF | 23.40 | 2.20 | |
| Pynn's Brook, NL, Canada (2015 to 2016) | OF | 19.98 | 4.21 | |
| | TF | 21.24 | 2.44 | |
| Salmon River, NL, Canada (2015 to 2016) | OF | 16.14 | 1.33 | |
| | TF | 21.00 | 2.65 | |
| Eagle River, NL, Canada (2015 to 2016) | OF | 11.59 | 0.53 | |
| | TF | 28.26 | 0.86 | |
| Mont St. Hilaire, QC, Canada (1987) | P | 2.00 | 0.49 | Dalva and Moore, 1991 |
| | TF | 12.13 | 2.05 | |
| | SF | 40.10 | 0.10 | |
| Northern China (2007 to 2008) | P | 2.4 to 3.9 | 1.4 to 2.7 | Pan et al., 2010 |
| Coulissenhieb, Northeast Bavaria (1995 to 1997) | P | 2.70 | - | Michalzik and Matzner, 1999 |
| | TF | 15.20 | - | |
| Hobcaw Barony, South Carolina, USA (2014 to 2015) | P | 1.20 | - | Chen et al., 2019 |
| | Pine TF | 26.00 | - | |
| | Oak TF | 38.8 | - | |
| University of Georgia, USA 2015 to 2016 | TF Epiphyte Oak | 17 | 23** | Van Stan et al., 2017 |
| | TF Bare Cedar | 20 | 32** | |
| | TF Epiphyte Cedar | 54 | 48** | |
| SMEARII Site, Southern Finland (1998 to 2012) | P | 3.24 | 2.32 | Pumpanen et al., 2014 |
| | TF | 10.10 | 4.35 | |

** Estimated DOC yield for 2016 (g C $m^{-2}$ $a^{-1}$) where sampled storms values (g C $event^{-1}$) were scaled to an annual deposition value using meteorological data and a linear rainfall-DOC yield relationship.

## 4.0 Conclusions and Future Directions

This paper presents a cost-effective automated deposition sampler for continuous collection of precipitation. An open-source procedure and schematics for building these samplers is provided alongside the rationale for selecting the materials in the current study to target analytes of scientific interest in wet deposition samples. These low-power systems are demonstrated in being capable of continuous off-grid use for sample collection over two years at the NL-BELT experimental sites, with replacement of battery power packs monthly or bimonthly, with on-grid

performance also provided for comparison. The resulting systems enhance the accessibility of automated wet deposition samplers to scientists globally and this work highlights their robust performance in collecting and preserving rainwater conductivity and pH, alongside providing measurements of DOC from this understudied region that builds a broader picture of the atmosphere-surface exchange of this biogeochemical pool across the NL-BELT. Comparability and complementariness of our results to well-established and current measurements of interest like DOC, demonstrate their efficacy **and potential application to the study of processes such as canopy-precipitation interactions through the collection of open fall and throughfall replicates.** The capacity to autonomously collect wet deposition, in addition to traditional bulk deposition samples can shed light on competing wet and dry deposition processes. Should on-grid capacity suit scientific objectives, these samplers are anticipated to be possible for use year-round when paired with more power-intensive strategies to facilitate solid to liquid phase transfer for detected and collected precipitation in the winter.

For the broader deposition-motivated community, the instrument design also allows for easy cost-effective modification of the number of replicate samplers, the material composition of all surfaces the aqueous samples interact with, as well as preservation strategies - depending on the analyte of interest. **For example, the lack of organic nitrogen measurements within universally established sampling and measurement procedures serves as a general example of the substantial knowledge gaps that may result when translating limited data sets to the wider global picture. This includes incomplete speciation and quantification across precipitation, aerosol, and gas phases. Monitoring systems that support U.S. deposition assessments (e.g., the NADP) only characterize the inorganic fraction of wet deposition. Additionally, modern emerging issues that require the continuation of existing deposition measurements or expansion of observation programs revolve around identifying and quantifying compound classes of concern, such as persistent organic pollutants. As reported in the literature, the deposition of these types of pollutants (e.g., polychlorinated biphenyls, polycyclic aromatic hydrocarbons, etc.) can be monitored using suitable collectors made of amber-coloured glass or stainless steel (Fingler et al., 1994; Amodio et al., 2014) - modifications which can be applied to the sample design detailed here. The samples collected in this work from this new instrumentation, specifically, are expected to be used further in several upcoming complementary and novel environmental monitoring studies. Not only will**

**this future work extend our biogeochemical analysis, but it will also assist in our studying of the transport of other anthropogenic pollutants of emerging interest which are beyond the scope of describing this new platform.**

*Data availability.* The data are available from the corresponding author (TV) on request.

*Author contributions.* AC, DP, and ML performed the data analysis. AC and DP wrote the manuscript with contributions from all authors. Sampler design and construction were led by TV, with assistance from BP and RH for initial prototypes, DP and ML for the revised iteration, and AC for the final modular control boards. Sample collection and associated characterization measurements were performed by BP and TV. Conceptualization and conduct of the sampling experiments were made by TV, CY, KE, and SZ. All authors were involved in examining and reviewing the results. All authors were involved in editing the paper.

*Competing interests.* The contact author has declared that none of the authors has any competing interests.

## 5.0 Acknowledgements

Funding for this work was provided by the Newfoundland and Labrador Department of Agrifoods and Forestry, Centre for Forestry Science and Innovation (Project 221269), and the Harris Centre at Memorial University. T. C. VandenBoer was supported for this work in-part through a Government of Canada Banting Postdoctoral Fellowship. Fieldwork sample collection by B. K. Place was supported by funding from Polar Knowledge Canada through the Northern Scientific Training Program. Additional financial support for full redesign of the samplers was provided through Environment and Climate Change Canada Grants & Contributions (GCXE20S009). A. A. Colussi acknowledges support for this work through a Natural Sciences and Engineering Research Council of Canada (NSERC) Graduate Scholarship – Master's program (CGSM) and Ontario Graduate Scholarship (OGS). M. Lao acknowledges support for this work through a NSERC Undergraduate Student Research Award (USRA). We thank C. M. Laprise and C. Conlan for aid in the collection and organization of samples for analysis, supported in part by the Memorial University Career Experience Program (MUCEP) and V. Sitahai through a York University Dean's Undergraduate Research Award (DURA). T. C. VandenBoer, C. J. Young and S. E. Ziegler were supported through the NSERC Discovery (RGPIN-2020-06166; RGPIN-2018-

05990; RGPIN-2018-05383) and Strategic Partnerships (479224) Programs. The authors would also like to thank B. Hearn, D. Harris, A. Skinner, C. Young, J. J. MacInnis, J. Warren, and L. Souza for their invaluable assistance in sampling site access and set up, off-season storage of collection units, sample collection and analysis, and meteorological reanalysis. We thank H. Hung and C. Shunthirasingham for productive discussions on modular design and considerations for collection of persistent pollutants.

## 6.0 References

Amodio, M., Catino, S., Dambruoso, P. R., de Gennaro, G., Di Gilio, A., Giungato, P., Laiola, E., Marzocca, A., Mazzone, A., Sardaro, A., and Tutino, M.: Atmospheric Deposition: Sampling Procedures, Analytical Methods, and Main Recent Findings from the Scientific Literature, Adv. Meteorol., 2014, 161730, https://doi.org/10.1155/2014/161730, 2014.

Argentino, C., Kalenitchenko, D., Lindgren, M., and Panieri, G.: HgCl2 addition to pore water samples from cold seeps can affect the geochemistry of dissolved inorganic carbon ([DIC], δ13CDIC), Mar. Chem., 251, 104236, https://doi.org/10.1016/j.marchem.2023.104236, 2023.

Arisci, S., Rogora, M., Marchetto, A., and Dichiaro, F.: The role of forest type in the variability of DOC in atmospheric deposition at forest plots in Italy, Environ. Monit. Assess., 184, 3415–3425, https://doi.org/10.1007/s10661-011-2196-2, 2012.

Audoux, T., Laurent, B., Desboeufs, K., Noyalet, G., Maisonneuve, F., Lauret, O., and Chevaillier, S.: Intra-event evolution of elemental and ionic concentrations in wet deposition in an urban environment, Atmospheric Chem. Phys., 23, 13485–13503, https://doi.org/10.5194/acp-23-13485-2023, 2023.

Avery, G. B., Willey, J. D., and Kieber, R. J.: Carbon isotopic characterization of dissolved organic carbon in rainwater: Terrestrial and marine influences, Atmos. Environ., 40, 7539–7545, https://doi.org/10.1016/j.atmosenv.2006.07.014, 2006.

Barber, V. P. and Kroll, J. H.: Chemistry of Functionalized Reactive Organic Intermediates in the Earth's Atmosphere: Impact, Challenges, and Progress, J. Phys. Chem. A, 125, 10264–10279, https://doi.org/10.1021/acs.jpca.1c08221, 2021.

Barrie, L. A. and Hales, J. M.: The spatial distributions of precipitation acidity and major ion wet deposition in North America during 1980, Tellus B Chem. Phys. Meteorol., 36, 333–355, https://doi.org/10.3402/tellusb.v36i5.14915, 1984.

Beverland, I. J., Heal, M. R., Crowther, J. M., and Srinivas, M. S. N.: Real-time measurement and interpretation of the conductivity and pH of precipitation samples, Water. Air. Soil Pollut., 98, 325–344, https://doi.org/10.1007/BF02047042, 1997.

Bowering, K. L., Edwards, K. A., Wiersma, Y. F., Billings, S. A., Warren, J., Skinner, A., and Ziegler, S. E.: Dissolved Organic Carbon Mobilization Across a Climate Transect of Mesic Boreal

Forests Is Explained by Air Temperature and Snowpack Duration, Ecosystems, 26, 55–71, https://doi.org/10.1007/s10021-022-00741-0, 2022.

Bowering, K. L., Edwards, K. A., and Ziegler, S. E.: Seasonal controls override forest harvesting effects on the composition of dissolved organic matter mobilized from boreal forest soil organic horizons, Biogeosciences, 20, 2189–2206, https://doi.org/10.5194/bg-20-2189-2023, 2023.

Bowyer, Peter J. (Ed.): Where the Wind Blows: A Guide to Marine Weather in Atlantic Canada, Breakwater Books Ltd., St John's, Newfoundland, 53 pp., 1995.

Boyd, C. E.: Carbon Dioxide, pH, and Alkalinity, in: Water Quality: An Introduction, edited by: Boyd, C. E., Springer International Publishing, Cham, 177–203, https://doi.org/10.1007/978-3-030-23335-8_9, 2020.

Brahney, J., Wetherbee, G., Sexstone, G. A., Youngbull, C., Strong, P., and Heindel, R. C.: A new sampler for the collection and retrieval of dry dust deposition, Aeolian Res., 45, 100600, https://doi.org/10.1016/j.aeolia.2020.100600, 2020.

Burkhardt, J. and Drechsel, P.: The synergism between SO2 oxidation and manganese leaching on spruce needles — A chamber experiment, Environ. Pollut., 95, 1–11, https://doi.org/10.1016/S0269-7491(96)00126-1, 1997.

Canadian Air and Precipitation Monitoring Network: Inspector's Reference Manual - Precipitation, 1985.

Cappellato, R., Peters, N. E., and Ragsdale, H. L.: Acidic atmospheric deposition and canopy interactions of adjacent deciduous and coniferous forests in the Georgia Piedmont, Can. J. For. Res., 23, 1114–1124, https://doi.org/10.1139/x93-142, 1993.

Carlson, J., Gough, W. A., Karagatzides, J. D., and Tsuji, L. J. S.: Canopy Interception of Acid Deposition in Southern Ontario, Can. Field-Nat., 117, 523–530, https://doi.org/10.22621/cfn.v117i4.799, 2003.

Casas-Ruiz, J. P., Bodmer, P., Bona, K. A., Butman, D., Couturier, M., Emilson, E. J. S., Finlay, K., Genet, H., Hayes, D., Karlsson, J., Paré, D., Peng, C., Striegl, R., Webb, J., Wei, X., Ziegler, S. E., and del Giorgio, P. A.: Integrating terrestrial and aquatic ecosystems to constrain estimates of land-atmosphere carbon exchange, Nat. Commun., 14, 1571, https://doi.org/10.1038/s41467-023-37232-2, 2023.

Cha, J.-Y., Lee, S.-C., Lee, E.-J., Lee, K., Lee, H., Kim, H. S., Ahn, J., and Oh, N.-H.: Canopy Leaching Rather than Desorption of PM2.5 From Leaves Is the Dominant Source of Throughfall Dissolved Organic Carbon in Forest, Geophys. Res. Lett., 50, e2023GL103731, https://doi.org/10.1029/2023GL103731, 2023.

Chen, H., Tsai, K.-P., Su, Q., Chow, A. T., and Wang, J.-J.: Throughfall Dissolved Organic Matter as a Terrestrial Disinfection Byproduct Precursor, ACS Earth Space Chem., 3, 1603–1613, https://doi.org/10.1021/acsearthspacechem.9b00088, 2019.

Ciruzzi, D. M. and Loheide, S. P.: Monitoring Tree Sway as an Indicator of Interception Dynamics Before, During, and Following a Storm, Geophys. Res. Lett., 48, e2021GL094980, https://doi.org/10.1029/2021GL094980, 2021.

Colli, M., Lanza, L. G., Rasmussen, R., and Thériault, J. M.: The Collection Efficiency of Shielded and Unshielded Precipitation Gauges. Part II: Modeling Particle Trajectories, J. Hydrometeorol., 17, 245–255, https://doi.org/10.1175/JHM-D-15-0011.1, 2016.

Coward, E. K., Seech, K., Carter, M. L., Flick, R. E., and Grassian, V. H.: Of Sea and Smoke: Evidence of Marine Dissolved Organic Matter Deposition from 2020 Western United States Wildfires, Environ. Sci. Technol. Lett., 9, 869–876, https://doi.org/10.1021/acs.estlett.2c00383, 2022.

Csavina, J., Field, J., Taylor, M. P., Gao, S., Landázuri, A., Betterton, E. A., and Sáez, A. E.: A review on the importance of metals and metalloids in atmospheric dust and aerosol from mining operations, Sci. Total Environ., 433, 58–73, https://doi.org/10.1016/j.scitotenv.2012.06.013, 2012.

Dalva, M. and Moore, T. R.: Sources and sinks of dissolved organic carbon in a forested swamp catchment, Biogeochemistry, 15, 1–19, https://doi.org/10.1007/BF00002806, 1991.

Di Lorenzo, R. A., Place, B. K., VandenBoer, T. C., and Young, C. J.: Composition of Size-Resolved Aged Boreal Fire Aerosols: Brown Carbon, Biomass Burning Tracers, and Reduced Nitrogen, ACS Earth Space Chem., 2, 278–285, https://doi.org/10.1021/acsearthspacechem.7b00137, 2018.

Dossett, S. R. and Bowersox, V. C.: National Trends Network Site Operation Manual, 1999.

Eaton, J. S., Likens, G. E., and Bormann, F. H.: Throughfall and Stemflow Chemistry in a Northern Hardwood Forest, J. Ecol., 61, 495–508, https://doi.org/10.2307/2259041, 1973.

Erisman, J. W. and Draaijers, G.: Deposition to forests in Europe: most important factors influencing dry deposition and models used for generalisation, Environ. Pollut., 124, 379–388, https://doi.org/10.1016/S0269-7491(03)00049-6, 2003.

Escarré, A., Carratalá, A., Àvila, A., Bellot, J., Piñol, J., and Milán, M.: Precipitation Chemistry and Air Pollution, in: Ecology of Mediterranean Evergreen Oak Forests, edited by: Rodà, F., Retana, J., Gracia, C. A., and Bellot, J., Springer Berlin Heidelberg, Berlin, Heidelberg, 195–208, https://doi.org/10.1007/978-3-642-58618-7_14, 1999.

Farmer, D. K., Boedicker, E. K., and DeBolt, H. M.: Dry Deposition of Atmospheric Aerosols: Approaches, Observations, and Mechanisms, Annu. Rev. Phys. Chem., 72, 375–397, https://doi.org/10.1146/annurev-physchem-090519-034936, 2021.

Feng, J., Vet, R., Cole, A., Zhang, L., Cheng, I., O'Brien, J., and Macdonald, A.-M.: Inorganic chemical components in precipitation in the eastern U.S. and Eastern Canada during 1989–2016: Temporal and regional trends of wet concentration and wet deposition from the NADP and CAPMoN measurements, Atmos. Environ., 254, 118367, https://doi.org/10.1016/j.atmosenv.2021.118367, 2021.

Fingler, S., Tkalčević, B., Fröbe, Z., and Drevenkar, V.: Analysis of polychlorinated biphenyls, organochlorine pesticides and chlorophenols in rain and snow, Analyst, 119, 1135–1140, https://doi.org/10.1039/AN9941901135, 1994.

Fowler, D.: Wet and Dry Deposition of Sulphur and Nitrogen Compounds from the Atmosphere, 1980.

Galloway, J. N. and Likens, G. E.: The collection of precipitation for chemical analysis, Tellus, 30, 71–82, https://doi.org/10.3402/tellusa.v30i1.10318, 1978.

Gao, S., Hegg, D. A., Hobbs, P. V., Kirchstetter, T. W., Magi, B. I., and Sadilek, M.: Water-soluble organic components in aerosols associated with savanna fires in southern Africa: Identification, evolution, and distribution, J. Geophys. Res. Atmospheres, 108, https://doi.org/10.1029/2002JD002324, 2003.

Gatz, D. F., Selman, R. F., Langs, R. K., and Holtzman, R. B.: An Automatic Sequential Rain Sampler, J. Appl. Meteorol. 1962-1982, 10, 341–344, 1971.

George, C.: Photosensitization is in the air and impacts the multiphase on oxidation capacity, 2023.

Germer, S., Neill, C., Krusche, A. V., Neto, S. C. G., and Elsenbeer, H.: Seasonal and within-event dynamics of rainfall and throughfall chemistry in an open tropical rainforest in Rondônia, Brazil, Biogeochemistry, 86, 155–174, https://doi.org/10.1007/s10533-007-9152-9, 2007.

Grennfelt, P., Engleryd, A., Forsius, M., Hov, Ø., Rodhe, H., and Cowling, E.: Acid rain and air pollution: 50 years of progress in environmental science and policy, Ambio, 49, 849–864, https://doi.org/10.1007/s13280-019-01244-4, 2020.

Guinotte, J. M. and Fabry, V. J.: Ocean Acidification and Its Potential Effects on Marine Ecosystems, Ann. N. Y. Acad. Sci., 1134, 320–342, https://doi.org/10.1196/annals.1439.013, 2008.

Hadiwijaya, B., Isabelle, P.-E., Nadeau, D. F., and Pepin, S.: Observations of canopy storage capacity and wet canopy evaporation in a humid boreal forest, Hydrol. Process., 35, e14021, https://doi.org/10.1002/hyp.14021, 2021.

Hall, D. J.: Precipitation collector for use in the Secondary National Acid Deposition Network, United States, 1985.

Han, G., Song, Z., Tang, Y., Wu, Q., and Wang, Z.: Ca and Sr isotope compositions of rainwater from Guiyang city, Southwest China: Implication for the sources of atmospheric aerosols and their seasonal variations, Atmos. Environ., 214, 116854, https://doi.org/10.1016/j.atmosenv.2019.116854, 2019.

Heald, C. L. and Kroll, J. H.: The fuel of atmospheric chemistry: Toward a complete description of reactive organic carbon, Sci. Adv., 6, https://doi.org/10.1126/sciadv.aay8967, 2020.

Heald, C. L., Gouw, J. de, Goldstein, A. H., Guenther, A. B., Hayes, P. L., Hu, W., Isaacman-VanWertz, G., Jimenez, J. L., Keutsch, F. N., Koss, A. R., Misztal, P. K., Rappenglück, B., Roberts, J. M., Stevens, P. S., Washenfelder, R. A., Warneke, C., and Young, C. J.: Contrasting Reactive Organic Carbon Observations in the Southeast United States (SOAS) and Southern California (CalNex), Environ. Sci. Technol., 54, 14923–14935, https://doi.org/10.1021/acs.est.0c05027, 2020.

Houle, D., Augustin, F., and Couture, S.: Rapid improvement of lake acid–base status in Atlantic Canada following steep decline in precipitation acidity, Can. J. Fish. Aquat. Sci., 79, 2126–2137, https://doi.org/10.1139/cjfas-2021-0349, 2022.

Howard, M., Hathaway, J. M., Tirpak, R. A., Lisenbee, W. A., and Sims, S.: Quantifying urban tree canopy interception in the southeastern United States, Urban For. Urban Green., 77, 127741, https://doi.org/10.1016/j.ufug.2022.127741, 2022.

Iavorivska, L., Boyer, E. W., and DeWalle, D. R.: Atmospheric deposition of organic carbon via precipitation, Acid Rain Its Environ. Eff. Recent Sci. Adv., 146, 153–163, https://doi.org/10.1016/j.atmosenv.2016.06.006, 2016.

Jacob, Daniel J.: Introduction to Atmospheric Chemistry, Princeton University Press, Princeton, New Jersey, 49 pp., 1999.

Jurado, E., Jaward, F. M., Lohmann, R., Jones, K. C., Simó, R., and Dachs, J.: Atmospheric Dry Deposition of Persistent Organic Pollutants to the Atlantic and Inferences for the Global Oceans, Environ. Sci. Technol., 38, 5505–5513, https://doi.org/10.1021/es049240v, 2004.

Jurado, E., Jaward, F., Lohmann, R., Jones, K. C., Simó, R., and Dachs, J.: Wet Deposition of Persistent Organic Pollutants to the Global Oceans, Environ. Sci. Technol., 39, 2426–2435, https://doi.org/10.1021/es048599g, 2005.

Kattner, G.: Storage of dissolved inorganic nutrients in seawater: poisoning with mercuric chloride, Mar. Chem., 67, 61–66, https://doi.org/10.1016/S0304-4203(99)00049-3, 1999.

Kirkwood, D. S.: Stability of solutions of nutrient salts during storage, Mar. Chem., 38, 151–164, https://doi.org/10.1016/0304-4203(92)90032-6, 1992.

Kochendorfer, J., Meyers, T. P., Hall, M. E., Landolt, S. D., and Diamond, H. J.: A new reference-quality precipitation gauge wind shield, Atmospheric Meas. Tech. Discuss., 2023, 1–17, https://doi.org/10.5194/amt-2023-2, 2023.

Kroll, J. H., Donahue, N. M., Jimenez, J. L., Kessler, S. H., Canagaratna, M. R., Wilson, K. R., Altieri, K. E., Mazzoleni, L. R., Wozniak, A. S., Bluhm, H., Mysak, E. R., Smith, J. D., Kolb, C. E., and Worsnop, D. R.: Carbon oxidation state as a metric for describing the chemistry of atmospheric organic aerosol, Nat. Chem., 3, 133–139, https://doi.org/10.1038/nchem.948, 2011.

Kuylenstierna, J. C., Rodhe, H., Cinderby, S., and Hicks, K.: Acidification in developing countries: ecosystem sensitivity and the critical load approach on a global scale., Ambio, 30, 20–28, https://doi.org/10.1579/0044-7447-30.1.20, 2001.

Laquer, F. C.: Sequential precipitation samplers: A literature review, Atmospheric Environ. Part Gen. Top., 24, 2289–2297, https://doi.org/10.1016/0960-1686(90)90322-E, 1990.

Laurent, B., Losno, R., Chevaillier, S., Vincent, J., Roullet, P., Bon Nguyen, E., Ouboulmane, N., Triquet, S., Fornier, M., Raimbault, P., and Bergametti, G.: An automatic collector to monitor insoluble atmospheric deposition: application for mineral dust deposition, Atmospheric Meas. Tech., 8, 2801–2811, https://doi.org/10.5194/amt-8-2801-2015, 2015.

Lawrence, C. E., Casson, P., Brandt, R., Schwab, J. J., Dukett, J. E., Snyder, P., Yerger, E., Kelting, D., VandenBoer, T. C., and Lance, S.: Long-term monitoring of cloud water chemistry at Whiteface Mountain: the emergence of a new chemical regime, Atmospheric Chem. Phys., 23, 1619–1639, https://doi.org/10.5194/acp-23-1619-2023, 2023.

Likens, G. E. and Butler, T. J.: Atmospheric Acid Deposition, in: The Handbook of Natural Resources, Atmosphere and Climate, vol. 6, edited by: Wang, Y., CRC Press, 2020.

Lin, W.-C., Brondum, K., Monroe, C. W., and Burns, M. A.: Multifunctional Water Sensors for pH, ORP, and Conductivity Using Only Microfabricated Platinum Electrodes, Sensors, 17, https://doi.org/10.3390/s17071655, 2017.

Lindberg, S. E., Lovett, G. M., Richter, D. D., and Johnson, D. W.: Atmospheric Deposition and Canopy Interactions of Major Ions in a Forest, Science, 231, 141–145, https://doi.org/10.1126/science.231.4734.141, 1986.

Lovett, G. M.: Atmospheric Deposition of Nutrients and Pollutants in North America: An Ecological Perspective, Ecol. Appl., 4, 629–650, https://doi.org/10.2307/1941997, 1994.

Lovett, G. M. and Kinsman, J. D.: Atmospheric pollutant deposition to high-elevation ecosystems, Atmospheric Environ. Part Gen. Top., 24, 2767–2786, https://doi.org/10.1016/0960-1686(90)90164-I, 1990.

Meteorological Service of Canada: 2004 Canadian Acid Deposition Science Assessment, , Library and Archives Canada, 2005.

Metzger, J. C., Schumacher, J., Lange, M., and Hildebrandt, A.: Neighbourhood and stand structure affect stemflow generation in a heterogeneous deciduous temperate forest, Hydrol. Earth Syst. Sci., 23, 4433–4452, https://doi.org/10.5194/hess-23-4433-2019, 2019.

Michalzik, B. and Matzner, E.: Dynamics of dissolved organic nitrogen and carbon in a Central European Norway spruce ecosystem, Eur. J. Soil Sci., 50, 579–590, https://doi.org/10.1046/j.1365-2389.1999.00267.x, 1999.

Moore, T. R.: Dissolved organic carbon in a northern boreal landscape, Glob. Biogeochem. Cycles, 17, https://doi.org/10.1029/2003GB002050, 2003.

Myers-Pigg, A. N., Louchouarn, P., Amon, R. M. W., Prokushkin, A., Pierce, K., and Rubtsov, A.: Labile pyrogenic dissolved organic carbon in major Siberian Arctic rivers: Implications for

wildfire-stream metabolic linkages, Geophys. Res. Lett., 42, 377–385, https://doi.org/10.1002/2014GL062762, 2015.

National Atmospheric Deposition Program: NADP Site Selection and Installation Manual, 2009.

Oka, A., Takahashi, J., Endoh, Y., and Seino, T.: Bark Effects on Stemflow Chemistry in a Japanese Temperate Forest I. The Role of Bark Surface Morphology, Front. For. Glob. Change, 4, https://doi.org/10.3389/ffgc.2021.654375, 2021.

Pacyna, J. M.: Ecological Processes: Atmospheric Deposition, in: Encyclopedia of Ecology, vol. 1, edited by: Jorgensen, S. E. and Fath, B. D., Elsevier Science, 275–285, 2008.

Pan, Y., Wang, Y., Xin, J., Tang, G., Song, T., Wang, Y., Li, X., and Wu, F.: Study on dissolved organic carbon in precipitation in Northern China, Atmos. Environ., 44, 2350–2357, https://doi.org/10.1016/j.atmosenv.2010.03.033, 2010.

Peden, M. E., Bachman, S. R., Brennan, C. J., Demir, B., James, K. O., Kaiser, B. W., Lockard, J. M., Rothery, J. E., Sauer, J., Skowron, L. M., and Slater, M. J.: Methods for collection and analysis of precipitation, 1986.

Pomeroy, J. W., Granger, R., Pietroniro, J., Elliott, J., Toth, B., and Hedstrom, N.: Classification of the Boreal Forest for Hydrological Processes, in: Proceedings of the Ninth International Boreal Forest Research Association Conference, 1999.

Pumpanen, J., Lindén, A., Miettinen, H., Kolari, P., Ilvesniemi, H., Mammarella, I., Hari, P., Nikinmaa, E., Heinonsalo, J., Bäck, J., Ojala, A., Berninger, F., and Vesala, T.: Precipitation and net ecosystem exchange are the most important drivers of DOC flux in upland boreal catchments, J. Geophys. Res. Biogeosciences, 119, 1861–1878, https://doi.org/10.1002/2014JG002705, 2014.

Ramanathan, V. and Carmichael, G.: Global and regional climate changes due to black carbon, Nat. Geosci., 1, 221–227, https://doi.org/10.1038/ngeo156, 2008.

Randall, David: An Introduction to the Global Circulation of the Atmosphere, Princeton University Press, Princeton, New Jersey, 43 pp., 2015.

Reddy, M. M., Liebermann, T. D., Jelinski, J. C., and Caine, N.: Variation in pH During Summer Storms Near the Continental Divide in Central Colorado, U.S.A.∗, Arct. Alp. Res., 17, 79–88, https://doi.org/10.1080/00040851.1985.12004450, 1985.

Richter, D. D. and Lindberg, S. E.: Wet Deposition Estimates from Long-Term Bulk and Event Wet-Only Samples of Incident Precipitation and Throughfall, J. Environ. Qual., 17, 619–622, https://doi.org/10.2134/jeq1988.00472425001700040017x, 1988.

Ryan, K. A., Adler, T., Chalmers, A., Perdrial, J., Shanley, J. B., and Stubbins, A.: Event Scale Relationships of DOC and TDN Fluxes in Throughfall and Stemflow Diverge From Stream Exports in a Forested Catchment, J. Geophys. Res. Biogeosciences, 126, e2021JG006281, https://doi.org/10.1029/2021JG006281, 2021.

Safieddine, S. A. and Heald, C. L.: A Global Assessment of Dissolved Organic Carbon in Precipitation, Geophys. Res. Lett., 44, 11,672-11,681, https://doi.org/10.1002/2017GL075270, 2017.

Saleh, R.: From Measurements to Models: Toward Accurate Representation of Brown Carbon in Climate Calculations, Curr. Pollut. Rep., 6, 90–104, https://doi.org/10.1007/s40726-020-00139-3, 2020.

Sanei, H., Outridge, P. M., Goodarzi, F., Wang, F., Armstrong, D., Warren, K., and Fishback, L.: Wet deposition mercury fluxes in the Canadian sub-Arctic and southern Alberta, measured using an automated precipitation collector adapted to cold regions, Atmos. Environ., 44, 1672–1681, https://doi.org/10.1016/j.atmosenv.2010.01.030, 2010.

Santín, C., Doerr, S. H., Kane, E. S., Masiello, C. A., Ohlson, M., de la Rosa, J. M., Preston, C. M., and Dittmar, T.: Towards a global assessment of pyrogenic carbon from vegetation fires, Glob. Change Biol., 22, 76–91, https://doi.org/10.1111/gcb.12985, 2016.

Siksna, R.: The electrolytical conductivity of precipitation water as an aid to the chemical analysis, Geofis. Pura E Appl., 42, 32–41, https://doi.org/10.1007/BF02113385, 1959.

Sleutel, S., Vandenbruwane, J., De Schrijver, A., Wuyts, K., Moeskops, B., Verheyen, K., and De Neve, S.: Patterns of dissolved organic carbon and nitrogen fluxes in deciduous and coniferous forests under historic high nitrogen deposition, Biogeosciences, 6, 2743–2758, https://doi.org/10.5194/bg-6-2743-2009, 2009.

Smith, W. H.: Air Pollution and Forests: Interactions Between Air Contaminants and Forest Ecosystems, 1st ed., Springer, New York, NY, 379 pp., 1981.

Stedman, J. R., Heyes, C. J., and Irwin, J. G.: A comparison of bulk and wet-only precipitation collectors at rural sites in the United Kingdom, Water. Air. Soil Pollut., 52, 377–395, https://doi.org/10.1007/BF00229445, 1990.

Stoddard, J. L., Jeffries, D. S., Lükewille, A., Clair, T. A., Dillon, P. J., Driscoll, C. T., Forsius, M., Johannessen, M., Kahl, J. S., Kellogg, J. H., Kemp, A., Mannio, J., Monteith, D. T., Murdoch, P. S., Patrick, S., Rebsdorf, A., Skjelkvåle, B. L., Stainton, M. P., Traaen, T., van Dam, H., Webster, K. E., Wieting, J., and Wilander, A.: Regional trends in aquatic recovery from acidification in North America and Europe, Nature, 401, 575–578, https://doi.org/10.1038/44114, 1999.

Stubbins, A., Silva, L. M., Dittmar, T., and Van Stan, J. T.: Molecular and Optical Properties of Tree-Derived Dissolved Organic Matter in Throughfall and Stemflow from Live Oaks and Eastern Red Cedar, Front. Earth Sci., 5, https://doi.org/10.3389/feart.2017.00022, 2017.

Thornton, M. M., Shrestha, R., Wei, Y., Thornton, P. E., Kao, S.-C., and Wilson, B. E.: Daymet: Monthly Climate Summaries on a 1-km Grid for North America, Version 4 R1, https://doi.org/10.3334/ORNLDAAC/2131, 2022.

Thornton, P. E., Running, S. W., and White, M. A.: Generating surfaces of daily meteorological variables over large regions of complex terrain, Aggreg. Descr. Land-Atmosphere Interact., 190, 214–251, https://doi.org/10.1016/S0022-1694(96)03128-9, 1997.

Thornton, P. E., Shrestha, R., Thornton, M., Kao, S.-C., Wei, Y., and Wilson, B. E.: Gridded daily weather data for North America with comprehensive uncertainty quantification, Sci. Data, 8, 190, https://doi.org/10.1038/s41597-021-00973-0, 2021.

United States Environmental Protection Agency: Integrated Science Assessment (ISA) for Oxides of Nitrogen, Oxides of Sulfur and Particulate Matter Ecological Criteria (Final Report, 2020), U.S. Environmental Protection Agency, Washington, DC, 2020.

Van Stan, J. T. and Stubbins, A.: Tree-DOM: Dissolved organic matter in throughfall and stemflow, Limnol. Oceanogr. Lett., 3, 199–214, https://doi.org/10.1002/lol2.10059, 2018.

Van Stan, J. T., Wagner, S., Guillemette, F., Whitetree, A., Lewis, J., Silva, L., and Stubbins, A.: Temporal Dynamics in the Concentration, Flux, and Optical Properties of Tree-Derived Dissolved Organic Matter in an Epiphyte-Laden Oak-Cedar Forest, J. Geophys. Res. Biogeosciences, 122, 2982–2997, https://doi.org/10.1002/2017JG004111, 2017.

VandenBoer, T. C.: AIM-IC: Applications to Nitrous Acid (HONO) in the Ambient Atmosphere and Precipitation Monitoring, Masters of Science, University of Toronto, 2009.

Vermette, S. J. and Drake, J. J.: Simplified wet-only and sequential fraction rain collector, Atmospheric Environ. 1967, 21, 715–716, https://doi.org/10.1016/0004-6981(87)90053-9, 1987.

Vet, R., Artz, R. S., Carou, S., Shaw, M., Ro, C.-U., Aas, W., Baker, A., Bowersox, V. C., Dentener, F., Galy-Lacaux, C., Hou, A., Pienaar, J. J., Gillett, R., Forti, M. C., Gromov, S., Hara, H., Khodzher, T., Mahowald, N. M., Nickovic, S., Rao, P. S. P., and Reid, N. W.: A global assessment of precipitation chemistry and deposition of sulfur, nitrogen, sea salt, base cations, organic acids, acidity and pH, and phosphorus, Glob. Assess. Precip. Chem. Depos. Sulfur Nitrogen Sea Salt Base Cations Org. Acids Acidity PH Phosphorus, 93, 3–100, https://doi.org/10.1016/j.atmosenv.2013.10.060, 2014.

Wang, X., Gemayel, R., Baboomian, V. J., Li, K., Boreave, A., Dubois, C., Tomaz, S., Perrier, S., Nizkorodov, S. A., and George, C.: Naphthalene-Derived Secondary Organic Aerosols Interfacial Photosensitizing Properties, Geophys. Res. Lett., 48, e2021GL093465, https://doi.org/10.1029/2021GL093465, 2021.

Washenfelder, R. A., Azzarello, L., Ball, K., Brown, S. S., Decker, Z. C. J., Franchin, A., Fredrickson, C. D., Hayden, K., Holmes, C. D., Middlebrook, A. M., Palm, B. B., Pierce, R. B., Price, D. J., Roberts, J. M., Robinson, M. A., Thornton, J. A., Womack, C. C., and Young, C. J.: Complexity in the Evolution, Composition, and Spectroscopy of Brown Carbon in Aircraft Measurements of Wildfire Plumes, Geophys. Res. Lett., 49, e2022GL098951, https://doi.org/10.1029/2022GL098951, 2022.

Wetherbee, G. A., Shaw, M. J., Latysh, N. E., Lehmann, C. M. B., and Rothert, J. E.: Comparison of precipitation chemistry measurements obtained by the Canadian Air and Precipitation

Monitoring Network and National Atmospheric Deposition Program for the period 1995–2004, Environ. Monit. Assess., 164, 111–132, https://doi.org/10.1007/s10661-009-0879-8, 2010.

Wonaschütz, A., Hersey, S. P., Sorooshian, A., Craven, J. S., Metcalf, A. R., Flagan, R. C., and Seinfeld, J. H.: Impact of a large wildfire on water-soluble organic aerosol in a major urban area: the 2009 Station Fire in Los Angeles County, Atmospheric Chem. Phys., 11, 8257–8270, https://doi.org/10.5194/acp-11-8257-2011, 2011.

Ziegler, S. E., Benner, R., Billings, S. A., Edwards, K. A., Philben, M., Zhu, X., and Laganière, J.: Climate Warming Can Accelerate Carbon Fluxes without Changing Soil Carbon Stocks, Front. Earth Sci., 5, https://doi.org/10.3389/feart.2017.00002, 2017.

*Supporting Information for*

# Cost Effective Off-Grid Automatic Precipitation Samplers for Pollutant and Biogeochemical Atmospheric Deposition

Alessia A. Colussi[1], Daniel Persaud[1], Melodie Lao[1], Bryan K. Place[2,‡], Rachel F. Hems[2,§], Susan E. Ziegler[3], Kate A. Edwards[4,ǂ], Cora J. Young[1,2], and Trevor C. VandenBoer[1,3]

[1] *Department of Chemistry, York University, Toronto, ON*
[2] *Department of Chemistry, Memorial University, St. John's, NL*
[3] *Department of Earth Science, Memorial University, St. John's, NL*
[4] *Canadian Forest Service, Natural Resources Canada, Corner Brook, NL*

[‡] Now at: *SciGlob Instruments & Services LLC, Columbia, MD, USA*
[§] Now at: *Department of Chemistry and Biochemistry, Oberlin College and Conservatory, OH, USA*
[ǂ] Now at*: Climate Change Impacts and Adaptation Division, Lands and Minerals Sector, Natural Resources Canada, Ottawa, ON*

**Correspondence:** Trevor VandenBoer (tvandenb@yorku.ca)

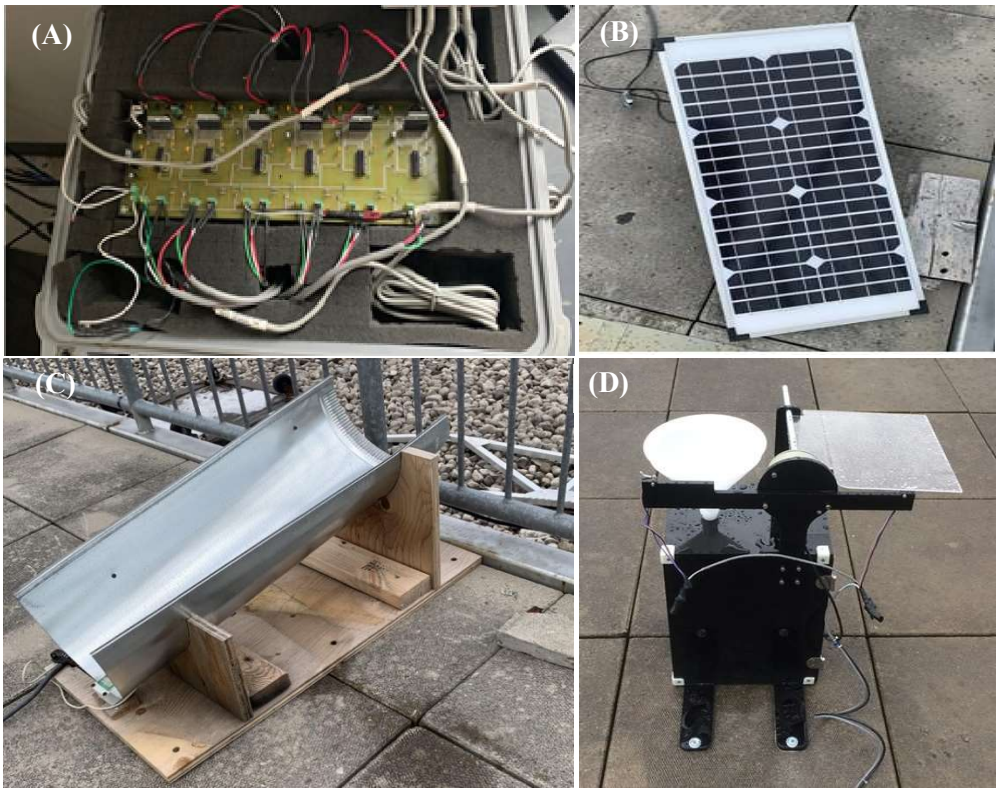


**Figure S1.** Automated precipitation array stationed at the Air Quality Research Station, York University, Toronto, consisting of: **(A)** weather-proofed control board, **(B)** 40 W solar panel, **(C)** rain sensor, and enhanced sensitivity chute, and **(D)** an automated collection unit fixed to concrete with lag sleeves and bolts during a rain event.

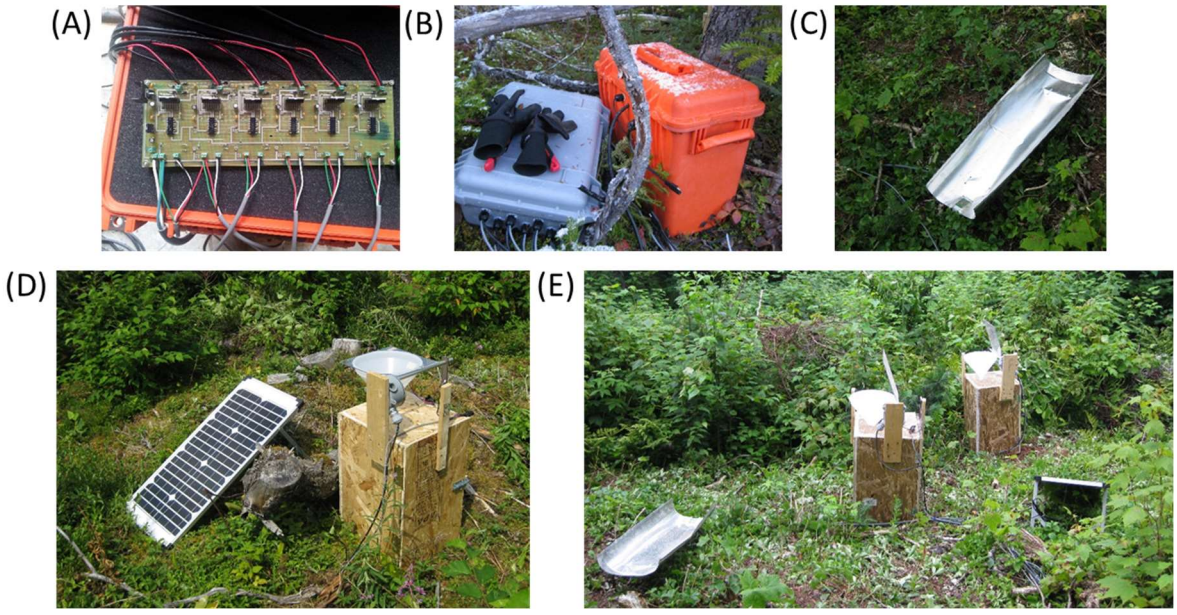


**Figure S2.** Automated precipitation samplers deployed at NL-BELT. The **(A)** weatherproof control board was powered by **(B)** an off-grid AGM battery. The **(C)** sensor chute modulated the

opening of the samplers for precipitation collection with **(D)** a 40 W solar panel to recharge the power package between **(E)** precipitation events when the lids open to collect wet deposition.

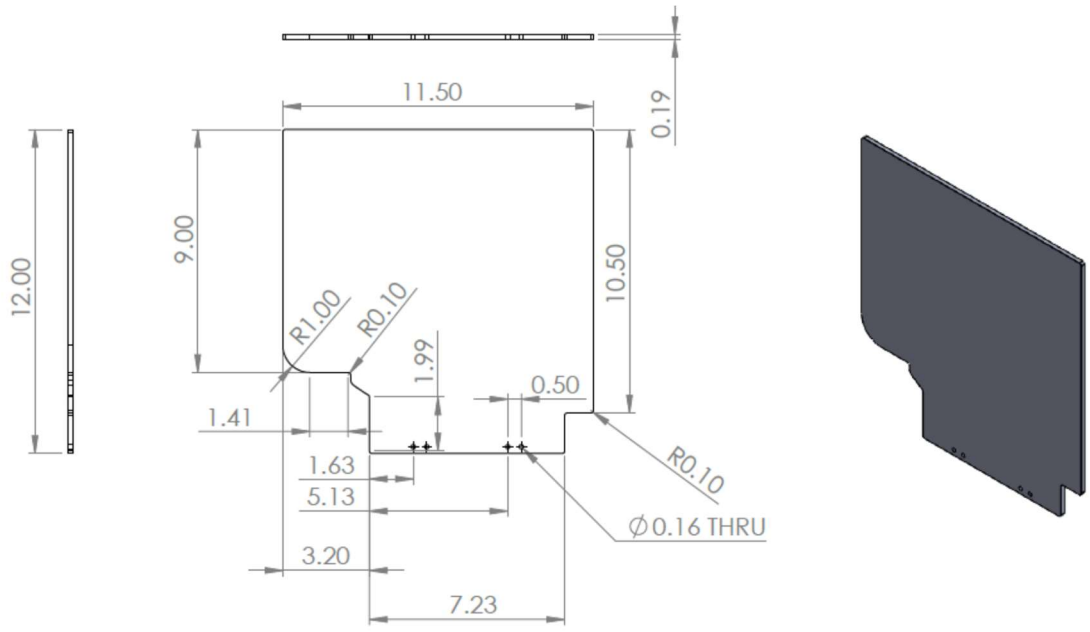


**Figure S3.** Dimensions (in inches) for automated collection unit lid, with mounting holes on the bottom edge to secure it to the aluminum lid rod.

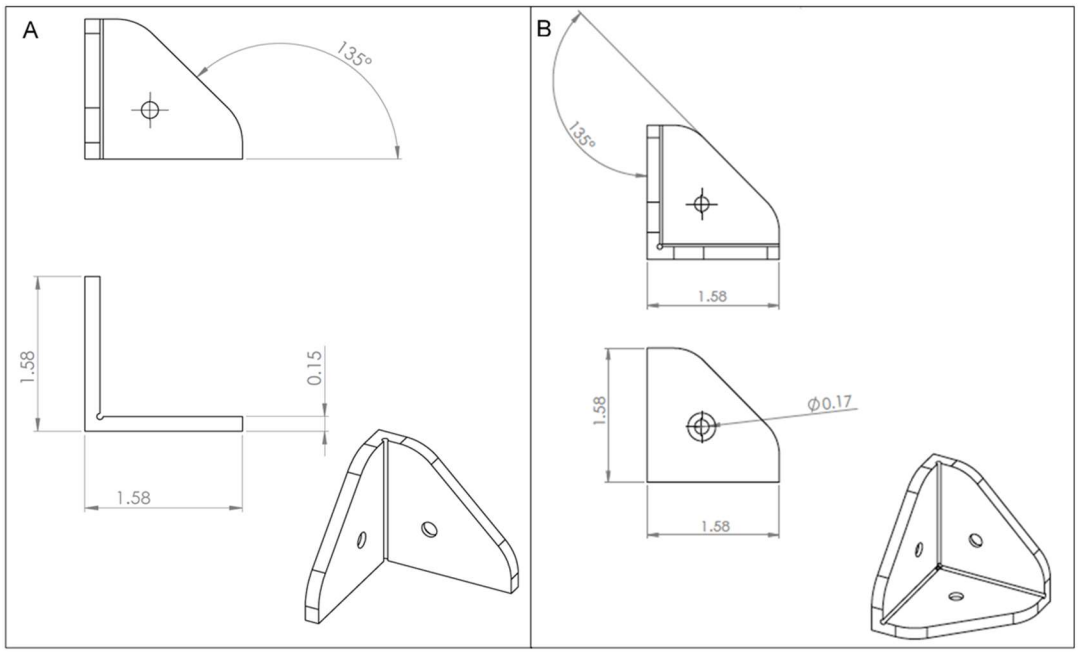

**Figure S4.** Dimensions (in millimeters) of 3D printed corner options: **(A)** double corner to affix panels adjoining the door and **(B)** multi corner used to secure three panels throughout the remainder of the collection unit.

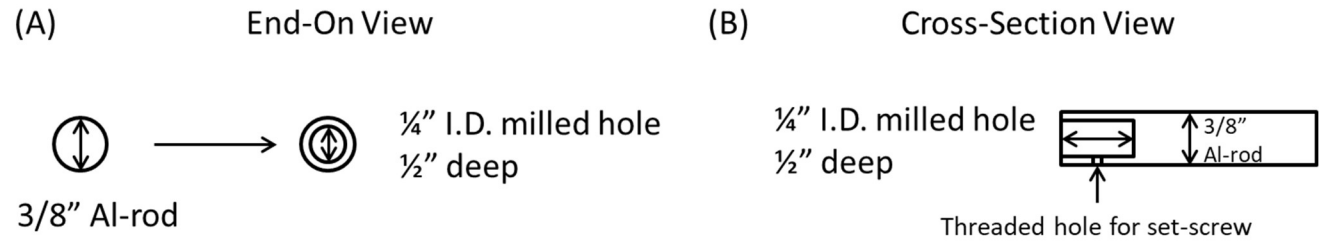


**Figure S5.** Aluminum rod milling schematics showing **(A)** end-on view for motor drive shaft and **(B)** cross section for situating the setscrew to hold the rod to the drive shaft of the motor.

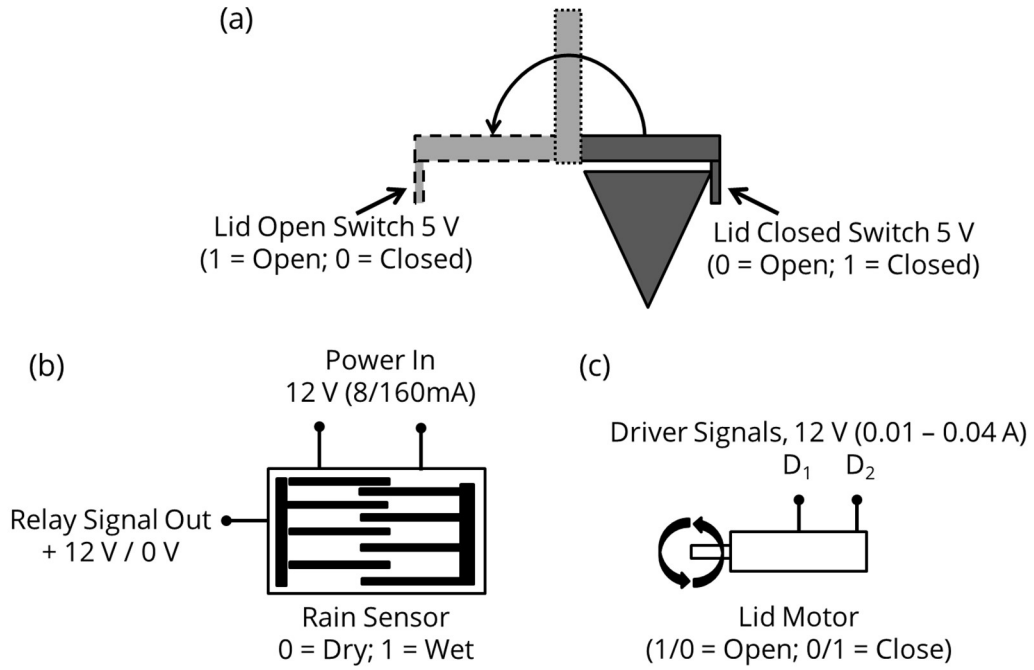


**Figure S6.** Voltage and logic states of the **(a)** lid switches, **(b)** precipitation sensor, and **(c)** lid motor used to drive digital decision making on custom control boards.

(a)

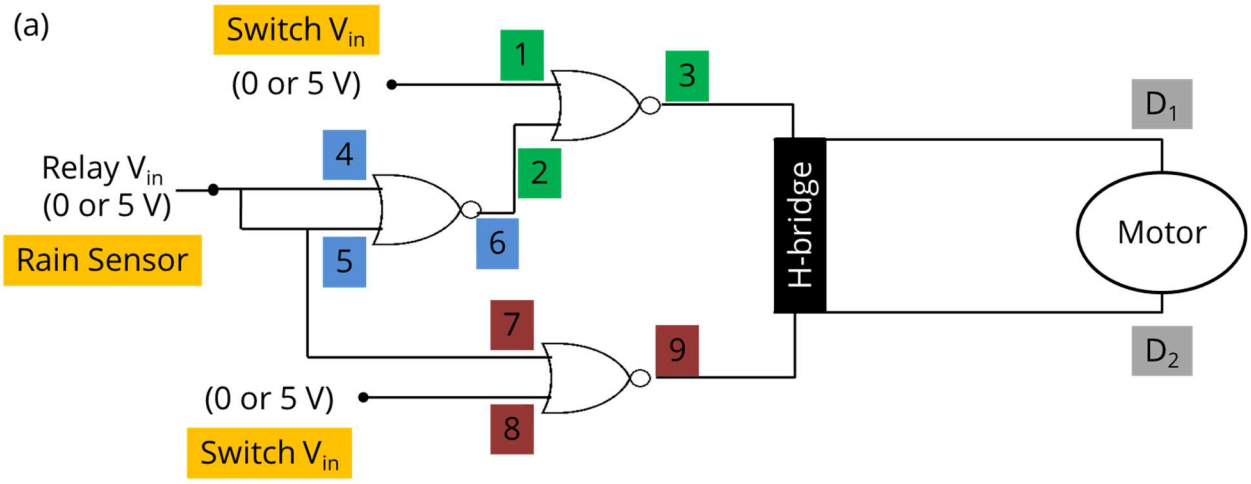


(b)

| Switch | Switch | Rain | 1 | 2 | 3 | 4 | 5 | 6 | 7 | 8 | 9 | D1 | D2 |
|---|---|---|---|---|---|---|---|---|---|---|---|---|---|
| 1 | 1 | 1 | X | X | X | X | X | X | X | X | X | X | X |
| 1 | 1 | 0 | X | X | X | X | X | X | X | X | X | X | X |
| 1 | 0 | 1 | 1 | 0 | 0 | 1 | 1 | 0 | 1 | 0 | 0 | 0 | 0 |
| 1 | 0 | 0 | 1 | 1 | 0 | 0 | 0 | 1 | 0 | 0 | 1 | 0 | 1 |
| 0 | 1 | 1 | 0 | 0 | 1 | 1 | 1 | 0 | 1 | 1 | 0 | 1 | 0 |
| 0 | 1 | 0 | 0 | 1 | 0 | 0 | 0 | 1 | 0 | 1 | 0 | 0 | 0 |
| 0 | 0 | 1 | 0 | 0 | 1 | 1 | 1 | 0 | 1 | 0 | 0 | 1 | 0 |
| 0 | 0 | 0 | 0 | 1 | 0 | 0 | 0 | 1 | 0 | 0 | 1 | 0 | 1 |

**Figure S7. (a)** Input layout for digital logic control of precipitation sampler using three NOR gates to operate a H-bridge motor driver and **(b)** corresponding truth table to input and output logic states for switches and rain sensor (yellow), first NOR gate (green), second NOR gate (blue), and third NOR gate (red) to control 12 VDC from the motor driver to the motor terminals ($D_1$ and $D_2$).

**S1. Measuring Conductivity Threshold of Kemo Electronic Rain Sensor.**

A simple procedure determined the conductivity threshold of the 12 VDC Kemo Electronic rain sensor. A 1000 µS/cm stock standard was prepared by dissolving 0.225 g of sodium chloride in 500 mL deionized water, ensuring thorough mixing for homogeneity. A series of conductivity standards were then prepared by diluting the stock standard with deionized water (DIW) to different levels near the suspected threshold of the sensor (0.75, 0.8, 0.9, 1.0, 2.0, 3.0, 4.0, and 5.0 µS/cm). Prior to this testing, the rain sensor was flushed with copious amount of DIW to remove any conductive substance from the surface of the sensor - this was also repeated in between trials. The result from testing with these solutions determined that the conductivity threshold for the relay is 1.0 µS/cm, as the rain sensor was observed to be only partially activated at 0.9 µS/cm and the result was not consistent.

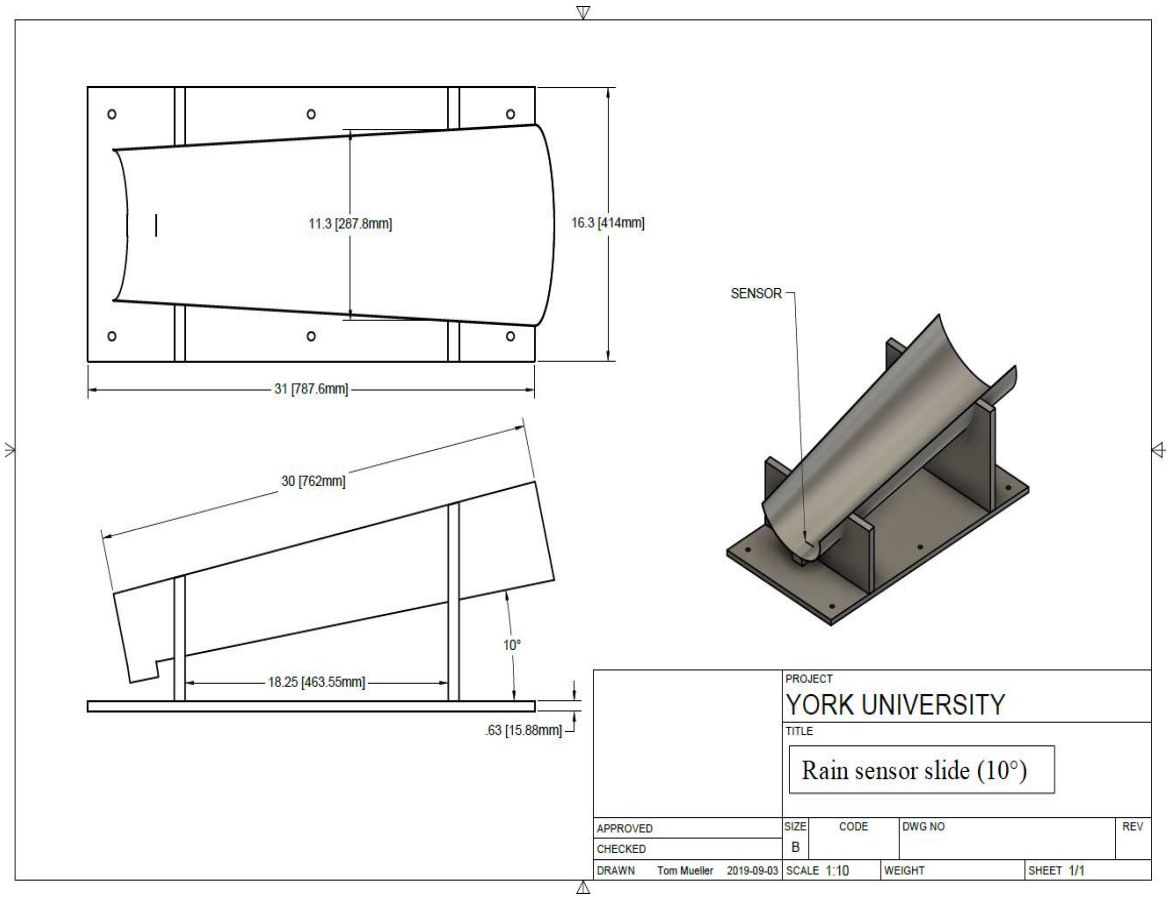


**Figure S8.** Design and dimensions (in mm) of the mounting chute for the rain sensor. The chute slope is fixed at an optimized angle of 10°, that maintains water on the surface of the sensor throughout a rain event but allows excess water to flow over the sensor when necessary. We also tested 15° and 20° through manual observation but found that rainwater would flow over the sensor too rapidly – limiting or even preventing detection of wet deposition events.

(a)

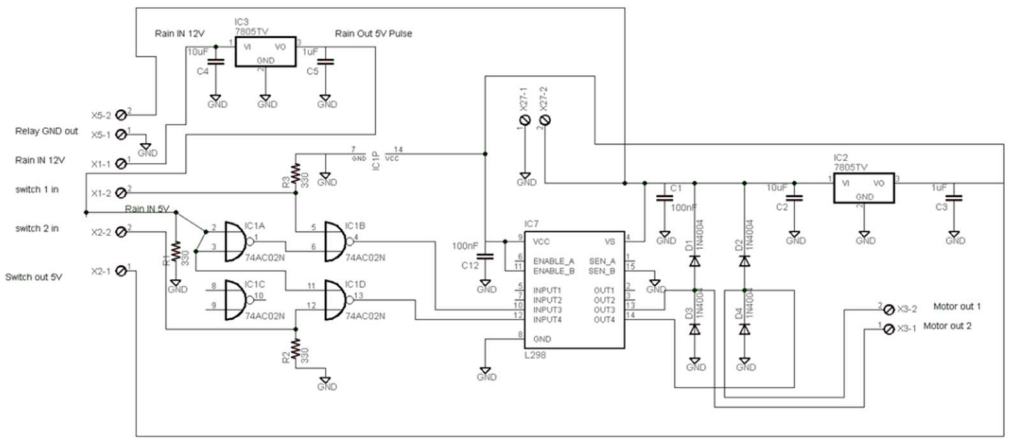


(b)

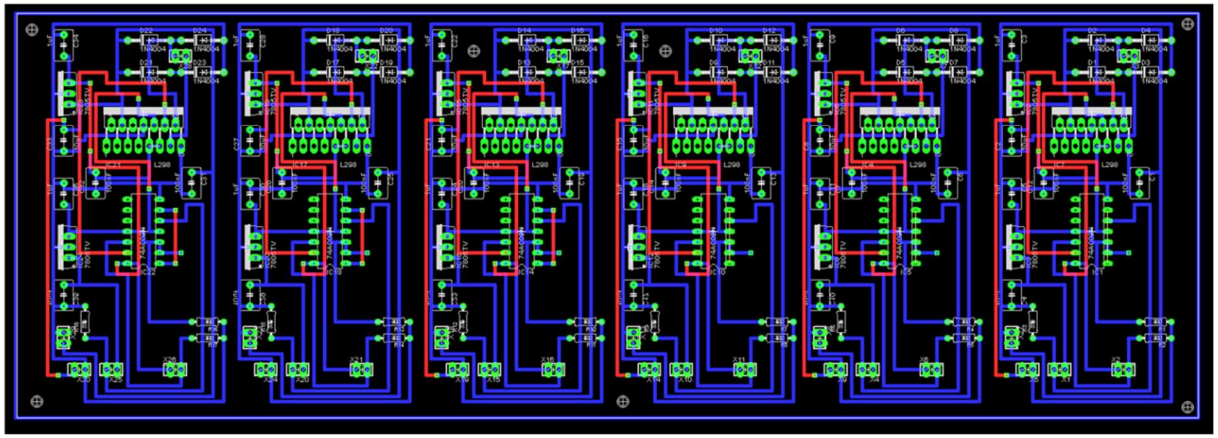

**Figure S9.** Technical schematics for all printed circuit board components required to control **(a)** one precipitation collector with all components and connections to chips indicated and **(b)** a complete six-unit array composed of replicate layouts.

**Table S1.** List of required components, part numbers, and quantities required to assemble a single printed circuit board.

| Component | Part Identification | Description | Quantity | Unit Price (CAD) |
|---|---|---|---|---|
| Integrated Circuit 1 (IC1) | 74AC02N = SN7402n | Four channels, two input NOR gate | 1 | 3.52 |
| Integrated Circuit 7(IC7) | L298N | Dual Full Bridge Driver | 1 | 7.41 |
| Integrated Circuit 2 (IC2), Integrated Circuit 3 (IC3) | 7805TV = MC7805CT-BP | 5V regulator, TO220 | 2 | 0.67 |
| Diode 1, Diode 2, Diode 3, Diode 4 | 1N4004 | Diode | 4 | 0.14 |
| Resistor 1, Resistor 2, Resistor 3 | 10k | resistor, %1, 1/4W | 3 | 0.21 |
| Capacitor 1, Capacitor 12 | 100nF cap | Capacitor, 0.1Uf / 50V | 2 | 0.35 |
| Capacitor 3, Capacitor 5 | 1Uf Cap | Capacitor, 1UF, 50V | 2 | 0.84 |
| Capacitor 2, Capacitor 4 | 10Uf | Capacitor, %10,10Uf,50V | 2 | 1.84 |

**Table S2.** List of specific components, manufacturers, and specifications required to construct precipitation collection arrays.

| Components | Description | Selection Rationale |
|---|---|---|
| | **Collection Units** | |
| Boxes | **Material:** 3/8" Acrylic or Plywood<br>**Dimensions:** (33.78 W x 33.78 L x 42.94 H) cm<br>See Figure 2 for more details | Acrylic and plywood were chosen for their low cost and durability against a variety of environmental conditions. Both materials are opaque to minimize light intrusion. |
| Collection Container | **Material:** High Density Polyethylene<br>**Brand:** Bel-Art Products<br>**Dimensions:** (19 H x 26 W x 36 H) cm; **Volume**: 10 L | Large volume collection of precipitation and resistance of material to environmental degradation. Quantitatively transfers analytes such as inorganic ions and DOC. |
| Funnel | **Material:** High Density Polyethylene<br>**Brand:** Dynalon<br>**Dimensions:** 9.4" W x 8.68" H; 20 cm diameter | Guides conductive precipitation into the collection container. Material is matched to maintain quantitative analyte transfer. |
| Sampler Lids | **Materials:** Lexan<br>**Brand:** Kraloy, Carlon® Lamson & Sessions<br>**Dimensions:** See Figure S3 for more details<br>**Voltage:** 12 V | Prevents foreign material entering the collection container when closed. Lexan was chosen due to its high flexibility and impact resistance. Acrylic was determined to be too fragile and not suitable for environmental conditions with elevated winds. |
| Geared Box DC Motor | **Brand:** Tsiny Motor Industrial Co. Ltd. TS-32GZ370-1650<br>**Operating voltage range**: 6-24 VDC<br>**Nominal voltage:** 12 VDC **Speed:** 2-8 RPM | The worm gear motor is connected to the aluminum rod and sampler lids to open and close them when conductive precipitation is detected by the rain sensor. |

**Table S2 (cont'd).** List of specific components, manufacturers, and specifications required to construct precipitation collection arrays.

| Components | Description | Selection Rationale |
|---|---|---|
| | **Collection Units (cont'd)** | |
| Lid Rod | **Material:** Aluminum<br>**Outer diameter:** 3/8"<br>**Inner diameter:** 1/4"<br>**Depth:** 1/2" deep | The aluminum rod is attached to the motor and facilitates the opening and closing of the Lexan lids. The rod is attached to the motor by a 8/32 threaded 1/4" set screw. |
| Lid Limit Switches | **Brand:** Omron Electronics<br>**Part Number:** D2FW-G271M(D)<br>**Max Current:** 1 A | Snap action switches are used to detect the open and closed position of the motorized sampler lids. Weatherproofing keeps them watertight. |
| Funnel Mesh | **Material:** HDPE<br>**Brand:** McMaster-Carr<br>**Part Number:** 9265T49 | When the automated sampler is in the open position, these cone-shaped filters prevent debris from entering the collection jug. |
| Lag shields, lag bolts and washers | **Lag shields dimensions:** 3/8" x 1-3/4"<br>(Requires masonry drill bit: 5/8")<br>**Lag bolt and washer dimensions:** 1/2" | These are utilized to secure precipitation collectors to concrete. This prevents unit tipping during storms or from animal interactions.<br>Tent pegs or rebar may be alternatively used to secure the samplers into soils. |
| | **Power System** | |
| Solar Panel | **Brand:** Coleman 40W Folding Panel<br>**Output Voltage:** 17.1 V, 2.3 amps<br>**Dimensions:** (79 L x 35.1 W x 1.8 H) cm | The solar panel recharges the off-grid battery. This can be repositioned to optimize sunlight exposure and maximize recharging capabilities. |

**Table S2 (cont'd).** List of specific components, manufacturers, and specifications required to construct precipitation collection arrays.

| Components | Description | Selection Rationale |
|---|---|---|
| | **Power System (cont'd)** | |
| Solar Charge Controller | **Brand:** Coleman<br>**Load Charge:** 8.5 A<br>**Cut-out:** 14.2 V<br>**Cut-in:** 13 V | The ability of the solar panel to deliver charge to the battery or stop when it is fully charged is regulated. The controller prevents the battery from overcharging. |
| 103 Ah off-grid battery | **Brand:** Motomaster Nautilus Ultra XD Group 31 High Performance AGM Deep Cycle Battery (103 Ah)<br>**Voltage:** 12 V<br>**Dimensions:** (33 L x 18 W x 25 H) cm | The 99.99% lead AGM (absorbed glass mat) was used for long lasting power and reliability for field testing without a solar panel. |
| 76 Ah Off-grid battery | **Brand:** Motomaster Nautilus Ultra XD Group 24 High Performance AGM Deep Cycle Battery (76 Ah)<br>**Voltage:** 12 V<br>**Dimensions:** (27.6 L x 17.1 W x 22.2 H) cm | The 99.99% lead AGM with 76 Ah battery was used for field testing while being charged with a solar panel for long periods. |
| Transformer | **Brand:** TDK Lambda Americas<br>**Voltage:** 115 VAC to 12 VDC | The transformer replaces an off-grid battery and converts 115 VAC to 12 VDC. This can be used when sampling in locations with grid power available. |

**Table S2 (cont'd).** List of specific components, manufacturers, and specifications required to construct precipitation collection arrays.

| Components | Description | Selection Rationale |
|---|---|---|
| | **Rain Detection** | |
| Heated Precipitation Sensor | **Brand:** Kemo Electronic M152<br>**Voltage:** 12 V<br>**Dimensions:** (6.5 x 4.5 x 3.6) cm | A waterproof conductive sensor that becomes activated and switches on a relay when in contact with conductive rain or snow. The sensor relay triggers the control board so that the sampler lids rotate open. **The operating temperature range provided by the manufacturer is -10 to +55°C.** |
| Sensor Chute | **Dimensions:** (see Figure S8) | Increases surface area of precipitation sensor to activate the relay. Delays lid closing by providing more conductive ions to the sensor surface when atmospheric wash out may occur. |
| | **Digital Control Board** | |
| Control Boards | See Figure S9 for more details. | Controls communication between the motors, power supply, and rain sensor (12 VDC), as well as the two limit switches (5 VDC). |
| Control Board Protective Case | **Brand:** Pelican ™ 1450 Case<br>**Material of body:** polypropylene<br>**Exterior Dimensions: (**41.8 L x 33 W x 17.3 D) cm<br>**Interior Dimensions:** (37.2 L x 26 W x 15.5 D) cm<br>**Weight with foam (polyurethane):** 2.9 kg | The 1450 case contains custom foam for cable accommodations with automatic pressure equalization valve to balance interior pressure. It is watertight, crushproof, and dustproof with double throw latches and a rubber handle. |
| Reusable Hydrosorbent Silica Gel Beads | **Brand:** Pelican Case Desiccant<br>**Canister Dimensions: (**1.3 L x 5.1 W x 10.2 H) cm<br>**Mass:** 40 g | The silica gel beads absorb moisture to prevent water damage to the control board; when clear, must reactivate in an oven for 3 hours at 300°F. |

**Table S2 (cont'd).** List of specific components, manufacturers, and specifications required to construct precipitation collection arrays.

| Components | Description | Selection Rationale |
|---|---|---|

## Miscellaneous

| | | |
|---|---|---|
| Data logger | **Brand**: ONSET® HOBO 4-channel analog data logger<br>**Part #:** UX120-006M<br>**Program:** HOBOware | To collect and offload data from the control board using one of four channels. This work: CH1 – battery voltage, CH2 – motor driver voltage, CH3 – rain sensor voltage, CH4 – limit switch voltage. |
| Cable Connectors | **Brand:** Bulgin (400 or 4000 Series Buccaneer) IP68 Sealed Electrical Circular Cable Connectors<br>PXP4010/03P/3540 and PSP4011/03S/3540<br>PSP4010/08P/3540 and PSP4011/08S/3540<br>SA3349, SA3350, SA3348, SA3347<br>**Material:** Polyamide UL94-V0 body, gold contacts<br>**Cable acceptance:** 3 mm – 7 mm<br>**Contact insertion:** crimp or solder | Waterproof and dustproof cable connectors provide electrical connections from the control board to the battery, solar panel, and sampler motors and switches. Different numbers of contacts represent different cable requirements within the system (2- or 3-contact = battery and solar panel cables, 6- or 8-contact = rain samplers). |
| Extension Cables | Any commercial outdoor-rated extension cord | To increase distance from VAC power source to sampling location. |

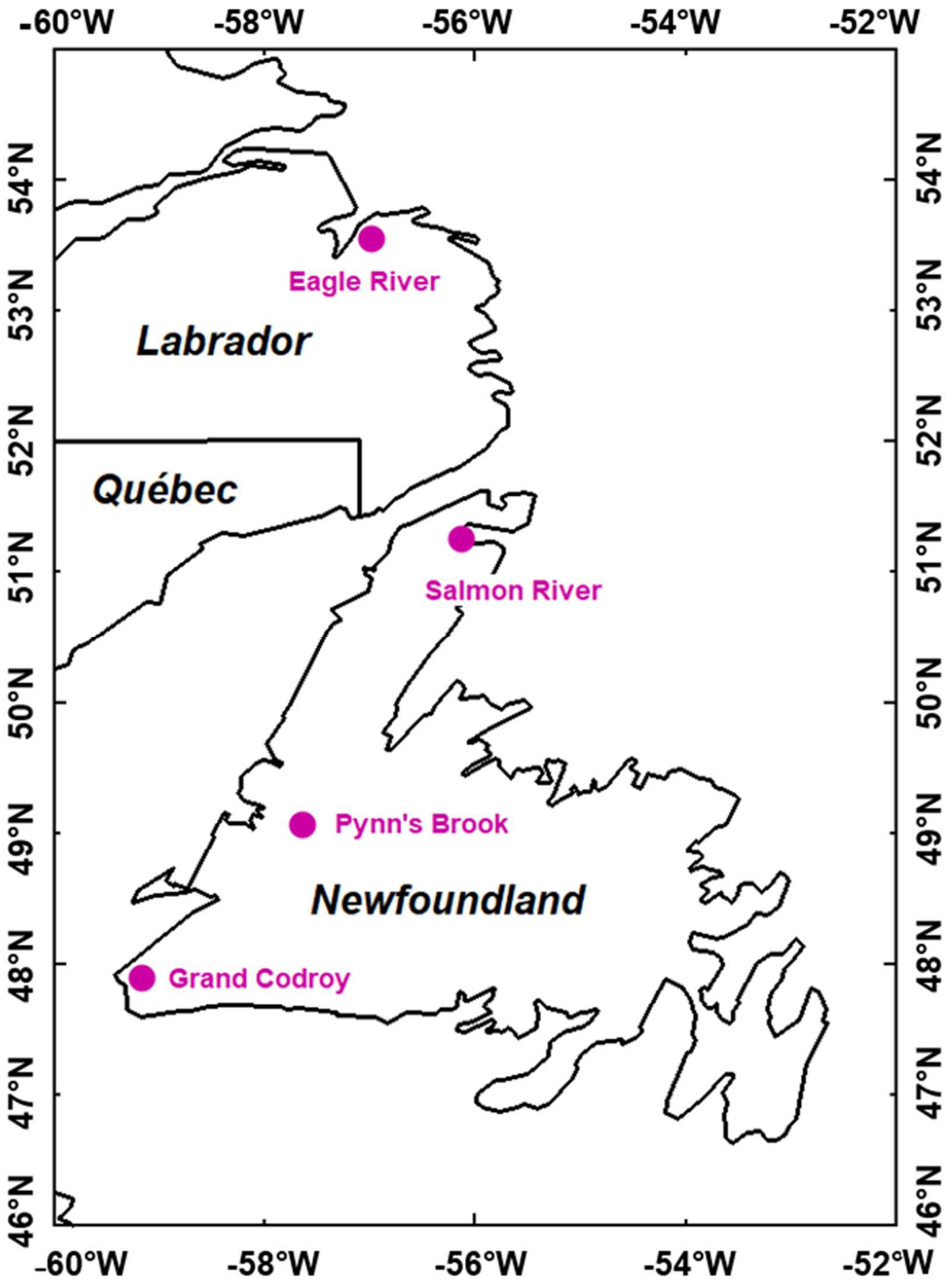


**Figure S10.** Map of the NL-BELT highlighting the four watershed regions where sampling occurred: Grand Codroy (GC), Pynn's Brook (PB), Salmon River (SR), and Eagle River (ER).

## S2. Deposition Comparison: This Work, DAYMET, and ECCC

Sufficiently continuous measurements from ECCC stations near each site are challenging to obtain for the 2015-16 period. When available with greater than 80% coverage, the ECCC datasets both agree and disagree with our observations in GC and SR, respectively, suggesting that there is substantial deposition volume heterogeneity at the scale of ~10 km in this region. In SR, the disagreement with our measurements is identical to the DAYMET model which uses ECCC observations as input data, while at GC the ECCC measurements are identical to ours (Table S3). Further, the discrepancy in the PB or ER average annual precipitation volume between ECCC and those of this work and DAYMET are not possible to interrogate due to the large quantity of data missing from the ECCC monitoring station (35.22% in ER and 39.65% in HR/PB; Table S3). The DAYMET observations are representative of a larger spatial scale, where our discrete samplers could be subject to heterogeneity in deposition (e.g., orographic precipitation, driven by topography like steep slopes) or impacted by meteorological conditions not captured by the model (e.g., undercatch driven by local winds). The temporally resolved volume comparisons at sampling interval timescales better-demonstrates comparability, despite the systematic differences. **The month-to-month relationships between DAYMET and our observations, as well as between ECCC and our observations, all show strong correlations with linear regressions having $R^2$ values, from north to south, of 0.72, 0.99, 0.99, and 0.86, and N/A, 0.94, N/A, and 0.93, respectively (Table S3)**. The discrepancy between DAYMET, ECCC, and our observations for total deposition were highest in the most northerly site, where the experimental site was located on a steep slope, with only 43 % of the predicted volume collected. At all of the sample collection sites on the island of Newfoundland, a consistent difference was observed with 65 ± 4 % of the estimated volume collected, except at GC where our measurements and those from ECCC are identical and starkly contrasting to DAYMET. Overall, parsing these comparisons is difficult and demonstrates that there may be up to 55% additional uncertainty in deposited species, should given measurements of a species be scaled for a watershed like ER by concentration in total deposition samples. We propose, that by isolating only the deposited analytes and using analyte fluxes instead of concentrations in precipitation samples, that uncertainty issues in representing volumes, improves overall deposition budget certainties.

**Table S3.** Collected precipitation volumes from NL-BELT in bulk deposition samplers for rainwater were deployed for one to two months, while snow was collected as an integrated sample throughout the winter because sites were not accessible. The Environment and Climate Change Canada (ECCC) precipitation data was obtained for identical sampling intervals. The DAYMET model for North America (1 km x 1 km resolution) for precipitation was obtained for the identical sampling intervals, which utilizes interpolated and extrapolated data from daily weather observations to predict inputs at the NL-BELT locations. Linear regression results for slope (m) and correlation coefficient ($R^2$) between observations and DAYMET (***italics***), and observations and ECCC (where possible; **underlined**), were calculated. For sampling periods where a measurement was compromised or not collected for a given interval in this work, these are reported as with '-' and an estimated volume from the regression relationship with ECCC is reported in parentheses when used to replace compromised samples.

| Date (mmm-yy) | Grand Codroy | | | Pynn's Brook/ Humber River | | | Salmon River | | | Eagle River | | |
|---|---|---|---|---|---|---|---|---|---|---|---|---|
| | This Work (L) | DAYMET (L) | ECCC (L) | This Work (L) | DAYMET (L) | ECCC (L) | This Work (L) | DAYMET (L) | ECCC (L) | This Work (L) | DAYMET (L) | ECCC (L) |
| Jun-15 | 22.68 | 40.98 | 23.80[b] | 23.44 | 36.94 | 11.47[b] | - | - | - | - | - | - |
| Jul-15 | 2.92 | 3.38 | 2.06 | 2.24 | 2.93 | 1.04[b] | 21.12 | 31.13 | 30.94 | 13.85 | 40.92 | 15.09[b] |
| Aug-15 | 6.86 | 8.08 | 7.20 | 5.06 | 6.86 | - | 1.89 | 4.71 | 9.52 | 3.66 | 6.96 | 2.64[c] |
| Sep-15 | (5.17)[a] | 2.93 | 5.17 | 3.05 | 4.70 | - | 5.29 | 6.62 | 6.44 | - | - | - |
| Oct-15 | 1.71 | 4.31 | 4.44 | - | - | - | 3.62 | 5.20 | 6.18 | - | - | - |
| Nov-15 | 3.57 | 5.92 | 4.92 | 5.66 | 8.61 | - | - | - | - | - | - | - |
| May-16 | 26.00 | 28.15 | 25.38 | 15.62 | 24.18 | 11.22[b] | 16.19 | 22.73 | 25.33 | - | - | - |
| Jun-16 | 1.83 | 4.21 | 3.79 | 4.25 | 4.51 | 2.79 | 2.39 | 3.11 | 3.05[a] | 22.94 | 45.68 | 22.70[b] |
| Jul-16 | 5.81 | 3.96 | 6.10 | 3.13 | 3.80 | 3.19 | 3.68 | 3.26 | - | - | - | - |
| Aug-16 | 5.19 | 4.10 | 3.98 | 4.67 | 6.14 | 4.23 | 3.60 | 5.18 | 3.89[a] | 5.82 | 10.79 | 6.94[b] |
| Sep-16 | 7.79 | 5.17 | 4.06 | 4.97 | 4.04 | - | 4.95 | 5.95 | 6.69 | - | - | - |
| Oct-16 | 5.10 | 6.69 | 5.30 | 5.15 | 5.84 | 3.47[b] | 2.00 | 2.82 | 2.58 | 5.42 | 8.32 | 4.39[b] |
| m, $R^2$ | 0.62, *0.859;* 1.02, 0.934 | | | 0.60, *0.990;* -, - | | | 0.68, *0.987;* 0.67, 0.941 | | | 0.43, *0.719;* -, - | | |

[a]Sample compromised by wildlife-sampler interaction.
[b]These values result from periods where <80% of the observation days report collected data. Partial volumes from the available data are presented.
[c]These values result from periods where <50% of the observation days report collected data. Partial volumes from the available data are presented.

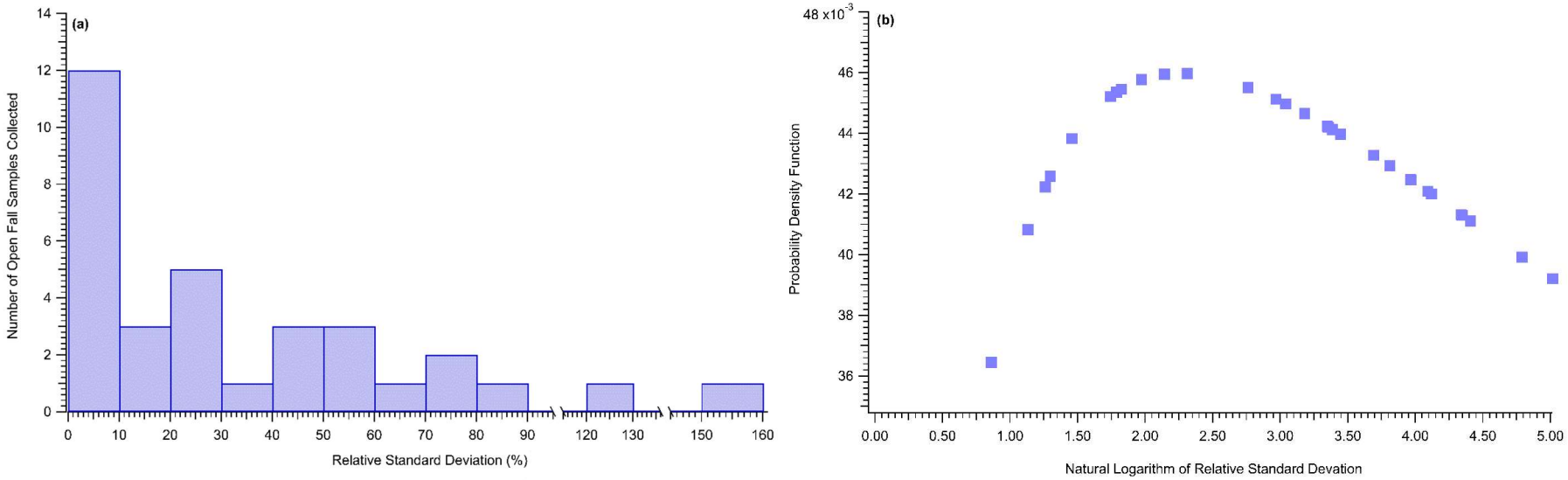


**Figure S11.** Thirty-three sets of triplicate open fall samples were collected across the NL-BELT between 2015 and 2016. **(a)** The replicate relative standard deviations (RSDs) appear to follow a log-normal distribution where reproducibility is typically within ± 12.5% and almost always within ± 31.5%. **(b)** A variable 'x' is said to have a lognormal distribution if y = ln(x) is normally distributed**.** The RSDs were treated as variable 'x' and then log-transformed, resulting in a mean (μ) and standard deviation (σ) of 2.81 and 1.41, respectively. The probability density function for the log-normal, plotted against these log-transformed values, is defined by the two parameters μ and σ, where x > 0. As a result, one of the 33 RSD values was excluded from this plot as it became a negative value after being log-transformed.

**Table S4.** Sum of DOC fluxes (mg C $m^{-2}$ $a^{-1}$) in wet deposition samples for 2015 and 2016 at GC, PB, SR, and ER. The average DOC flux error (mg C $m^{-2}$ $a^{-1}$) propagated by summing the errors across the sampling sites to obtain the annual values.

| | | OF | TF |
|---|---|---|---|
| **Site** | **Year** | **Deposition Flux (mg C $m^{-2}$ $a^{-1}$)** | |
| GC | 2015 | 1800 (± 800) | 3700 (± 2400) |
| | 2016 | 1400 (± 800) | 700 (± 700) |
| PB | 2015 | 600 (± 300) | 1800 (± 600) |
| | 2016 | 7800 (± 7700) | 3000 (± 3600) |
| SR | 2015 | 2000 (± 900) | 3500 (± 2000) |
| | 2016 | 4000 (± 1700) | 1700 (± 1500) |
| ER | 2015 | 100 (± 100) | 1600 (± 2200) |
| | 2016 | 1000 (± 800) | 100 (± 30) |

**Table S5.** Average DOC flux (mg C $m^{-2}$ $a^{-1}$) for 2015 to 2016 at GC, PB, SR, and ER. The difference between calculated fluxes in TF and OF samples are also included.

| | OF | TF | TF - OF |
|---|---|---|---|
| **Site** | **Flux (mg C $m^{-2}$ $a^{-1}$)** | | |
| GC | 1600 | 2200 | 600 |
| PB | 4200 | 2400 | -1800 |
| SR | 3000 | 2600 | 400 |
| ER | 500 | 900 | 400 |